Regulation of macroautophagy and microautophagic lipophagy by phosphatidylserine synthase Cho1 and external ethanolamine

Nanaru Mineoka[1], Rikako Konishi[1], Yuri Nakashima[1], Moe Muramoto[1], Kayoko Fukuda[1], Sayuri Kuriyama[1], Tatsunori Masatani[2,3], Akikazu Fujita[1,*]

[1]Department of Molecular and Cell Biology and Biochemistry, Basic Veterinary Science, Faculty of Veterinary Medicine, Kagoshima University, Korimoto 1-21-24, Kagoshima 890-0065, Japan

[2]Laboratory of Zoonotic Diseases, Faculty of Applied Biological Sciences, Gifu University, 1-1 Yanagido, Gifu 501-1193, Japan

[3]Center for One Medicine Innovative Translational Research (COMIT), Gifu University, 1-1 Yanagido, Gifu 501-1193, Japan

***Corresponding author:**

Akikazu Fujita

Department of Molecular and Cell Biology and Biochemistry, Basic Veterinary Science, Faculty of Veterinary Medicine, Kagoshima University, Korimoto 1-21-24, Kagoshima 890-0065, Japan

Tel/Fax: +81 99 285 8714

E-mail: afujita@vet.kagoshima-u.ac.jp

Abstract

Phospholipids play crucial roles in autophagy; however, the underlying mechanisms remain elusive. We previously found that the phosphatidylserine (PtdSer) transporter Osh5 is critical for autophagosome formation. Therefore, in this study, we aimed to investigate the impact of the knockout of *cho1*, which encodes PtdSer synthase, on autophagy. Green fluorescent protein-autophagy-related gene 8 (GFP-Atg8) processing assay revealed a significant defect in the macroautophagic activity of the *cho1*Δ mutant, regardless of the presence or absence of ethanolamine (Etn). Notably, autophagosomes were absent in the cytosol, and macroautophagic bodies were not observed in the vacuoles of the starved *cho1*Δ mutant, underscoring the essential role of PtdSer synthesized using Cho1 in autophagosome biogenesis. In contrast, numerous microautophagic vesicles containing lipid droplets were observed in the vacuoles of *cho1*Δ mutants starved in the presence of Etn, suggesting the crucial role of phosphatidylethanolamine (PtdEtn) synthesized via the Kennedy pathway in microautophagic lipophagy when PtdSer synthesis using Cho1 is disrupted. Given recent evidence pointing to the involvement of the ubiquitination system in various autophagy-related processes, we also examined the role of ubiquitin-conjugating enzyme E2 gene *ubc4*. Moreover, microautophagic lipophagy was significantly diminished in starved *cho1*Δ yeast with *ubc4* knockout. These findings suggest the critical role of Ubc4-mediated ubiquitination in facilitating microautophagic lipophagy of the vacuole in yeast cells.

Keywords: Phospholipid, Electron microscopy, Rapid freezing, Freeze-fracture, Ubiquitination

46 **Abbreviations**

47 BSA, bovine serum albumin

48 CDP, cytidine diphosphate

49 DAG, diacylglycerol

50 EF, E-face (exoplasmic leaflet)

51 EM, electron microscopy

52 ESCRT, endosomal sorting complex required for transport

53 Etn, ethanolamine

54 GFP, green fluorescent protein

55 GST, glutathione S-transferase

56 HRP, horse radish peroxidase

57 IMP, intra-membrane particle

58 ORF, open reading frame

59 Osh, oxysterol-binding protein homologue

60 PBS, phosphate-buffered saline

61 PF, P-face (protoplasmic or cytoplasmic leaflet)

62 PH, pleckstrin homology

63 PtdEtn, phosphatidylethanolamine

64 PtdSer, phosphatidylserine

65 PtdIns(3)P, phosphatidylinositol 3-phosphate

66 PtdIns(4)P, phosphatidylinositol 4-phosphate

67 PtdIns(4,5)P_2, phosphatidylinositol 4,5-bisphosphate

68 QF, quick-freezing

69 QF-FRL, quick-freezing and freeze-fracture replica labeling

70 RT-PCR, reverse transcription-polymerase chain reaction

71 SDS, sodium dodecyl sulfate

72 YPD, yeast peptone dextrose

73 WT, wild-type

1. Introduction

Autophagy involves various systems that transport cytoplasmic components into lysosomes (vacuoles) and perform many physiological and pathological functions [1]. The three main types of autophagy distinguished by their morphological and mechanistic characteristics are macroautophagy, microautophagy, and chaperone-mediated autophagy [1]. Each type involves the delivery of cargo to the lysosomes (vacuoles), where the acidic environment and acid hydrolases break down their contents into basic components for subsequent anabolic processes. Macroautophagy, the most extensively studied form of autophagy, involves the formation of double-membrane vesicles, called autophagosomes, which sequester cellular components. More than 30 autophagy-related genes (ATGs) regulate different stages of autophagy, such as nucleation, orientation, and elongation of the autophagosome and its fusion with the lysosome (vacuole) [2]. In contrast, mechanisms of microautophagy, involving direct invagination of the lysosomal (vacuolar) membrane to engulf the target cargo [3-5], remain unclear.

Lipids are crucial to sustain life, as they are the key components of biological membranes and metabolic energy reserves, contributing significantly to various signaling pathways. Lipids, particularly phospholipids, are also crucial primary membrane sources for the phagophore or isolation membrane and involved in membrane elongation during autophagosome formation in macroautophagy [6-8] and in the expansion of the vacuole membrane during microautophagic lipophagy [9, 10]. In macroautophagy, phospholipid transport by Atg2 [6, 11] and its scrambling by Atg9 [7, 8] are crucial for autophagosome biogenesis. Furthermore, inner membrane (in mammals) or macroautophagic body membrane (in yeast) of the double-membrane

98 structure of the autophagosome undergoes selective degradation after fusion with the
99 lysosome or vacuole [12]. Therefore, phospholipid components are modulated during
100 autophagosome maturation before and during fusion with the target organelles [13-15].
101 However, the specific types of phospholipids localized or required at each stage of
102 autophagy remain unknown.

103 Phospholipid distribution in the plasma and intracellular membranes has
104 mainly been studied using fluorescently tagged protein domains binding to hydrophilic
105 head groups of phospholipids in the cytoplasm [16-18]. However, overexpression of
106 these phospholipid-binding protein domains interferes with the membrane recruitment
107 of authentic phospholipid effectors and inhibits phospholipid-dependent cellular
108 processes [19, 20]. For example, overexpression of phosphatidylinositol 3-phosphate
109 (PtdIns(3)P)-binding probes, such as the 2xFYVE domain of EEA1 or PX domain of
110 p40phox, to visualize PtdIns(3)P blocks phagosome maturation at an early stage [21],
111 thus interfering with the analysis of the PtdIns(3)P content of late phagosomes or
112 phagolysosomes. Additionally, this method does not provide information on
113 phospholipid distribution in the luminal leaflets of organelle membranes. Electron
114 microscopy (EM) using ultrathin sections generally detects some lipids in both leaflets
115 [22-24], but it cannot determine the exact location of the lipids in the luminal or
116 cytoplasmic leaflet owing to section thickness and low membrane contrast. Therefore,
117 we previously used the quick-freeze and freeze-fracture replica labeling (QF-FRL)
118 method, which facilitates nanoscale membrane lipid labeling by physically fixing the
119 membrane molecules [13, 25-27]. This technique is particularly important to analyze
120 autophagosomes, in which the double-membranes are closely apposed, and vesicle
121 structures, such as macroautophagic bodies, within the vacuole lumen.

We previously investigated the roles of Osh proteins homologous to oxysterol-binding proteins, which mediate non-vesicular lipid transport, in macroautophagy in yeast [15]. We found that macroautophagic activity was significantly impaired in the *osh1-osh7*Δ: *osh4*^{ts} mutant. Additionally, using the QF-FRL method, we found that autophagosomes were absent from the cytoplasm of the mutant. Among the *osh* gene-deletion mutants, *osh5*Δ mutant exhibited a defect in macroautophagic activity, with a notable absence of cytoplasmic autophagosomes. Furthermore, autophagosomes in the *osh5*Δ mutant were smaller, with noticeably thinner inner and outer membranes, compared to those in wild-type (WT) yeast. Labeling density of phosphatidylserine (PtdSer) in the autophagosome membrane of the *osh5*Δ mutant was also significantly lower than that in the autophagosome membrane of WT yeast [15]. These findings indicated the crucial role of PtdSer in autophagosome biogenesis. PtdSer is synthesized using the Cho1 enzyme in yeast cells. In this study, we aimed to further examine the specific roles of PtdSer synthesized using Cho1 in macroautophagy.

Here, our study revealed that PtdSer synthesized using Cho1 was essential for macroautophagy and autophagosome biogenesis in yeast cells. Additionally, exogenously supplied ethanolamine (Etn) induced microautophagic lipophagy in the vacuole of the starved *cho1*Δ mutant, indicating that phosphatidylethanolamine (PtdEtn) synthesized via the Kennedy pathway is essential for the microautophagic lipophagy. Furthermore, our results suggest the essential role of the ubiquitin-conjugating E2 enzyme Ubc4 in microautophagic lipophagy.

143 **2. Methods**

144 ***2.1. Probes***

145 Complementary DNA (cDNA) generated by RT-PCR of HEK293 cell total RNA was
146 used as a template to clone the PX domain of p40Phox and PH domains of OSBP. The
147 plasmid containing the PHx2 domain of Evectin-2 was kindly provided by Dr.
148 Tomohiko Taguchi (Touhoku University) and Dr. Takuma Kishimoto (Hokkaido
149 University). Recombinant GST fusion proteins containing, the PX domain of p40Phox
150 (GST-p40Phox-PX), OSBP PH domain (GST-OSBP-PH), Evectin-2 PH domain (GST-
151 Evectin-2-PH), and phospholipase C (PLC)-δ1 PH domain (GST-PLCδ1-PH) were
152 expressed in *Escherichia coli* and purified as previously described [14, 27, 28]. The PH
153 domain of PLC-δ1 was obtained from the GST-PLC-PH domain fusion protein via
154 cleavage with PreScission protease (GE Healthcare Life Sciences, Pittsburgh, PA, USA)
155 according to the manufacturer's protocol. The secondary rabbit anti-GST antibody was
156 purchased from Bethyl Laboratories (Montgomery, TX, USA). 10 nm gold particle-
157 conjugated anti-mouse IgG and anti-rabbit IgG antibodies were purchased from BioCell
158 (Cardiff, UK) and Jackson ImmunoResearch (West Grove, PA, USA). Biotin-
159 conjugated duramycin-LC (biotin-duramycin), and mouse anti-biotin antibody were
160 purchased from Polysciences (Warrington, PA, USA), and Jackson ImmunoResearch
161 Laboratories (West Grove, PA, USA), respectively. Rabbit monoclonal anti-GFP
162 antibody (Cell Signaling Technology, Danvers, U.S.A.) and HRP-linked anti-rabbit IgG
163 antibody (Cytiva, Tokyo, Japan) were used for western blotting analysis.

164

165 ***2. 2. Cultivation of yeast cells***

166 Yeast cells were grown in YPD medium (1% yeast extract, 2% Bacto Peptone and 2%

167 dextrose) or SMD (synthetic minimal medium; 0.67% yeast nitrogen base without
168 amino acids, 2% glucose) at 30 °C, and were harvested during the transition from
169 exponential or stationary phase. All yeast strains used in this study were based on the
170 parent strain *Saccharomyces cerevisiae* SEY6210 (*MATAα leu2-3, 112 ura3-52 his3-*
171 *Δ200 trp1-Δ901 lys2-801 suc2Δ9 GAL*) [29] (Table S1). Deletion mutants were
172 generated using a polymerase chain reaction (PCR)-based method with pUG6, pAG32,
173 and pFA6a-TRP1 plasmids as templates [30]. To induce autophagy, cells cultured in
174 YPD medium were washed with water and incubated for 3–5 h at 30 °C in nitrogen and
175 carbon-deleted medium S(-NC) (0.17% yeast nitrogen base without amino acids and
176 ammonium sulfate (Bacton Dickinson), nitrogen-depleted medium SD(-N) (0.17% yeast
177 nitrogen base without amino acids and ammonium sulfate and 2% dextrose) or carbon-
178 depleted medium SN(-C) (1% yeast extract and 2% Bacto Peptone). S(-NC), SD(-N)
179 and SN(-C) mediums were supplemented with 1 mM phenylmethylsulfonyl fluoride
180 (PMSF, Sigma) when needed.
181
182 ***2. 3. Plasmids***
183 The plasmid pRS316-GFP-ATG8 [31] was provided by the National BioResource
184 Project, Japan.
185
186 ***2. 4. Macroautophagic activity assay***
187 Macroautophagic activity was assessed by monitoring the degradation of GFP-tagged
188 Atg8 within vacuoles, following the method described by Cheong et al. [32].
189
190 ***2. 5. Quick-freezing and freeze–fracture electron microscopy***

191 Quantitative lipid labeling of the biological membranes of budding yeast cells was
192 performed by quick-freezing yeast cells using either a metal sandwich method or high-
193 pressure freezing using an HPM 010 high-pressure freezing machine (Leica
194 Microsystems, Wetzlar, Germany). For metal sandwich freezing, a small volume of
195 yeast pellet was placed on a copper foil, covered with a thin gold foil (~4 mm^2 in area;
196 20 μm thick), and frozen using a quick press between two gold-plated copper blocks
197 precooled in liquid nitrogen [28, 33]. For high-pressure freezing, an EM grid (200
198 mesh) impregnated with yeast cells was sandwiched between a flat aluminum disc
199 (Engineering Office M. Wohlwend, Sennwald, Switzerland) and frozen according to the
200 manufacturer's instructions [34].
201 For freeze–fracture, frozen specimens were transferred to a cold stage of a
202 Balzers BAF400 apparatus (Bal-Tec AG, Lichtenstein) and fractured at −130 °C under a
203 vacuum of ~1×10^{-6} millibars. Replicas were prepared by electron-beam evaporation in
204 three steps: carbon (C) (~2-nm-thick) at an angle of 90° to the specimen surface,
205 platinum–carbon (Pt/C; 1–2 nm) at an angle of 45°, and C (10–20 nm) at an angle of
206 90°, as previously described [25]. The thickness of the deposit was adjusted using a
207 crystal-thickness monitor (EM QSG100, Leica).
208 Thawed specimens were incubated with 2.5% sodium dodecyl sulfate (SDS)
209 in 0.1 M Tris–HCl (pH 8.0) at 60 °C to 70 °C overnight. To remove the cell wall, yeast
210 replicas were digested with 1 mg/mL Zymolyase 20T in phosphate-buffered saline
211 (PBS) containing 0.1% Triton X-100, 1% bovine serum albumin (BSA), and a protease
212 inhibitor cocktail (Nacalai Tesque) for 2 h at 37 °C. After further treatment with 2.5%
213 SDS, the replicas were stored in buffered 50% glycerol at –30 °C until use.
214

215 ***2. 6. Labeling and electron microscopy observation***

216 Probe labeling was performed as described previously [25]. Briefly, after rinsing,
217 freeze-fracture replicas were blocked with PBS containing 2% cold-water fish skin
218 gelatin at room temperature for 30 min. To label PtdIns(3)P, PtdIns(4)P, and PtdSer, the
219 samples were incubated at 4 °C overnight with 30 μg/mL GST-p40Phox-PX, 40 μg/mL
220 GST-OSBP-PH, or 20 μg/mL GST-Evectin2-PH in PBS containing 2% cold-water fish
221 skin gelatin, respectively. Then, the samples were successively incubated in PBS
222 containing 2% cold-water fish skin gelatin at 37 °C for 30 min each with rabbit anti-
223 GST antibody (5 μg/mL) and 50-fold diluted colloidal gold (10 nm)-conjugated anti-
224 rabbit IgG antibody (EM.GFAR 10; BBI Solutions, Cardiff, UK). To block the
225 nonspecific binding of GST-OSBP-PH to PtdIns(4,5)P_2, the replicas were pretreated
226 with the PH domain (1 mg/mL) of PLC-δ1 in a blocking solution [28]. To label PtdEtn,
227 biotin-duramycin (60 μM) was diluted in PBS containing 2% cold-water fish skin
228 gelatin. After four washes with PBS containing 0.1% BSA, replicas were incubated at
229 37 °C for 30 min with mouse anti-biotin antibody (130 μg/ml), followed by incubation
230 with 10 nm gold-conjugated anti-mouse IgG antibody (Jackson ImmunoResearch, West
231 Grove, PA, USA) in PBS containing 2% cold-water fish skin gelatin.

232

233 ***2. 7. Statistical Analysis***

234 Each experiment was repeated at least three times. The areas on the images were
235 measured using Fiji (ImageJ), and the labeling density was indicated as the number of
236 colloidal gold particles in 1 μm^2. For each structure, the labeling density was measured
237 in more than 10 randomly selected images. Statistical differences between samples were
238 tested using *t*-test or Dunnett's multiple tests.

3. Results

3. 1. Defects in macroautophagic activity and autophagosome formation in the cho1 deletion mutant

To observe macroautophagic membranes, yeast cells were cultured for 5 hours in S(-NC) medium supplemented with PMSF, which is devoid of nitrogen and carbon sources. This condition was chosen for subsequent experiments as it robustly induces macroautophagy, facilitating frequent observation of larger autophagosomes [35]. In agreement with previous studies [34, 36], freeze-fracture EM revealed autophagosomes in yeast as spherical structures surrounded by double smooth membranes (Fig. 1A) [37]. The outer and inner membranes of autophagosomes were clearly distinguishable based on the convexity/concavity of their structure and their relative positions within the double membrane (Fig. 1A). Smooth-surfaced macroautophagic bodies were also identified within the vacuolar lumen (blue and green in Fig. 1B), consistent with the notion that these structures are derived from the inner autophagosomal membrane. In autophagy-deficient mutants lacking genes such as ATG2, ATG3, ATG5, ATG7, ATG8, ATG9, ATG12, ATG16, ATG18, VPS15, or VPS34, neither autophagosomes nor macroautophagic bodies were observed as we previously reported [36]. Similar results were obtained when macroautophagy was induced by nitrogen starvation using SD(-N) medium [36] or carbon starvation using SD(-Dextrose) medium (unpublished data, [38]) in the presence of PMSF. Moreover, macroautophagic bodies were largely absent from the vacuoles of yeast cells starved in S(-NC) medium without PMSF, consistent with prior observations [15]. In contrast, they accumulated markedly in the vacuoles of *pep4*Δ and *atg15*Δ mutants under the same conditions, even in the absence of PMSF, as previously reported [14]. These findings suggest that macroautophagic bodies are

263 normally degraded by vacuolar proteinases and lipases. We previously reported that the
264 vacuoles of starved WT yeast predominantly contain two types of vesicles—
265 macroautophagic bodies and microautophagic vesicles—arising from macroautophagy
266 and microautophagic lipophagy, respectively [9, 10, 14]. However, distinguishing
267 between them based on morphological features is challenging, as both vesicle types
268 exhibit smooth surfaces and similar sizes when observed using the freeze-fracture EM
269 method (see Figs. 1B, 2A). As reported previously [14], our quick-freezing and freeze-
270 fracture replica labeling (QF-FRL) method revealed that PtdIns(3)P was localized in
271 both the PF (cytoplasmic leaflet, see Supplemental Fig. S1) and EF (luminal leaflet) of
272 yeast autophagosomal membranes (Fig. 1A). Labelling of PtdIns(3)P was significantly
273 stronger in the EF of both the inner and outer membranes. Additionally, PtdIns(3)P was
274 intensively labeled in the membranes of macroautophagic bodies, showing a similar
275 luminal leaflet (EF)-dominant asymmetry (Figs. 1B, and S2). These findings support the
276 hypothesis that macroautophagic bodies are derived from the inner autophagosomal
277 membrane (Supplementary Fig. S3), which predominantly features PtdIns(3)P in its EF
278 (Supplementary Fig. S4). In contrast to macroautophagic bodies, we and other groups
279 previously reported that PtdIns(3)P is localized in the PF, but not EF, in
280 microautophagic vesicles in the vacuole caused by microautophagic lipophagy (see
281 Figs. 2 and S2) [10, 14].
282 The ULK complex (Atg1 in yeast) and FIP200 (Atg11 and Atg17 in yeast) play
283 a central role in autophagy initiation by assembling on the ER membrane, a critical hub
284 for phospholipid synthesis required for autophagosome formation [39]. Notably, FIP200
285 has been observed to colocalize with key enzymes involved in phospholipid
286 biosynthesis, such as phosphatidylserine synthase 1 (PSS1) and phosphatidylinositol

287 synthase (PIS). PIS synthesizes phosphatidylinositol (PI), which serves as a precursor
288 for PtdIns(3)P [40] and PtdIns(4)P [36, 41], both of which are indispensable for
289 macroautophagy. Additionally, our previous findings demonstrated that the
290 macroautophagic activity was significantly impaired in the *osh1-osh7*Δ: *osh4*^{ts} mutant,
291 which lacks functional PtdSer transporters. The cytoplasmic abundance of
292 autophagosomes was markedly reduced in the *osh5*Δ mutant, and PtdSer labeling in
293 autophagosome membranes was substantially lower compared to WT yeast, if
294 detectable at all [15]. These results suggest that PtdSer itself or its metabolic
295 derivatives, synthesized by Cho1, likely play a pivotal role in the regulation of
296 macroautophagy in budding yeast.
297 To explore the role of Cho1, the PtdSer synthase, in macroautophagy, we
298 analyzed the macroautophagic membranes of *cho1*Δ mutants using freeze-fracture EM.
299 We found in this study that the appearance rate of autophagosomes in the cytoplasm was
300 significantly lower in starved *cho1*Δ mutants, regardless of the presence or absence of
301 Etn, compared to the WT strain (Fig. 1C). Moreover, macroautophagic bodies were
302 absent in the vacuoles of the starved *cho1*Δ mutants (Figs. 2C and 3D). Atg8, a
303 ubiquitin-like protein crucial for autophagosome formation, relies on its conjugation to
304 PtdEtn for association with autophagosomal membranes [42, 43]. In yeast, PtdEtn is
305 primarily synthesized through two pathways: from PtdSer via Psd1 [44, 45] or Psd2
306 [46], and via the cytidine diphosphate (CDP)-Etn (Kennedy) pathway [47]
307 (Supplementary Fig. S5). Additionally, minor pathways contribute to PtdEtn synthesis
308 in yeast [48]. In this study, freeze-fracture EM showed that autophagosomes were
309 present in the cytoplasm of starved WT yeast cells, both with and without Etn (Fig. 1C).
310 Similarly, the marked difference in autophagosome formation

311 between *cho1*Δ and *psd1*Δ/*psd2*Δmutants indicates that the presence of PtdSer itself,
312 rather than its conversion to downstream metabolites, is crucial for autophagosome
313 formation and macroautophagy (Fig. 1C). Macroautophagic bodies were also detected
314 in the vacuoles of both starved WT and *psd1*Δ/*psd2*Δ strains in S(-NC)
315 medium containing PMSF, regardless of Etn supplementation (Figs. 2 and 3D). These
316 observations indicate that PtdEtn synthesized via both the major and minor pathways is
317 sufficient for Atg8 conjugation. However, the results highlight that PtdSer, synthesized
318 by the Cho1 enzyme, is indispensable for autophagosome formation.
319 Atg8, a ubiquitin-like protein, is conjugated to PtdEtn and remains associated
320 with mature autophagosomes as described above. During macroautophagy, green
321 fluorescent protein (GFP)-tagged Atg8 is degraded in the vacuoles, leading to the
322 release of free GFP. The presence of a relatively stable GFP component serves as an
323 indicator of macroautophagy. We confirmed the deficiencies of the macroautophagy in
324 the *cho1*Δ mutant using this GFP-Atg8 processing assay. Here, we did not detect free
325 GFP under nutrient-rich conditions. However, after cultured the cells in the S(-NC)
326 medium without PMSF for 4 h, a distinct band of free GFP was visible in WT yeast
327 (Fig. 1D). In this study, normal macroautophagic activity was observed in WT yeast
328 cells starved in S(-NC) medium in the absence of Etn (Fig. 1D). Furthermore,
329 *psd1*Δ/*psd2*Δ mutant exhibited comparable macroautophagic activity to WT yeast in
330 both the presence and absence of Etn (Fig. 1D). These results align with a previous
331 report [49], which found no detectable defects in the macroautophagic activity of
332 starved *psd1*Δ and *psd2*Δ mutants, suggesting that alternative PtdEtn synthesis pathways
333 can compensate for the loss of specific pathways. In contrast, a significantly lower
334 amount of free GFP was observed in the *cho1*Δ strain than in the WT strain (Fig. 1D),

335 indicating a significant deficiency in macroautophagy in the *cho1*Δ mutant in both the
336 presence and absence of Etn (Fig. 1D). Similar results were obtained in all strains
337 starved by nitrogen starvation using SD(-N) medium for 4 h (Supplementary Fig. S6).
338 These results are consistent with the observation obtained with the freeze-fracture EM
339 method.
340
341 ***3. 2. Microautophagic lipophagy in the starved cho1Δ mutant***
342 In the starved *cho1*Δ mutant, no vesicular structures were detected in the
343 vacuole lumen using the freeze-fracture EM method when starvation was induced in S(-
344 NC) containing PMSF in the absence of Etn (Fig. 2Ca). However, many vesicular
345 structures were observed in the vacuole lumen of the starved *cho1*Δ mutant in the
346 presence of Etn (Fig. 2Cb). As described above, the QF-FRL method revealed that
347 PtdIns(3)P is predominantly localized in EF of the macroautophagic body (Fig. 1B),
348 which originates from the inner vesicle of the autophagosome, in the vacuole
349 (Supplementary Fig. S3). In this study, we detected PtdIns(3)P labeling in the PF, but
350 not in EF, of the vesicular membranes within the vacuole lumen (Fig. 2Cb) of the *cho1*Δ
351 mutant starved in the presence of Etn, indicating that these vesicular structures are not
352 identical to the macroautophagic bodies. Moreover, several macroautophagic bodies, in
353 which the PtdIns(3)P labeling was predominantly detected in EF, but not in PF, were
354 detected in the vacuoles of WT yeast and *psd1*Δ/*psd2*Δ mutant starved in the absence
355 and presence of Etn (Fig. 2A, B, and D). In addition to PtdIns(3)P, PtdEtn labeling was
356 detected in both the EF and PF of the autophagosomes (Fig. 3A) and macroautophagic
357 bodies (Fig. 3Ba) of starved WT yeast. Labeling densities of PtdEtn were not
358 significantly different between the EF and PF of the autophagosome in the cytoplasm

359 (Fig. 3A, C) and macroautophagic bodies in the vacuole (Fig. 3Ba, C) of starved WT
360 yeast. However, PtdEtn labeling was localized in PF, but not in EF, of the vesicles in the
361 vacuolar lumen of the *cho1*Δ mutant starved in the presence of Etn (Fig. 3Bb and C).
362 Labeling density of PtdEtn in PF was significantly higher than that in EF of the vesicles
363 in the vacuolar lumen of the starved *cho1*Δ mutant in the presence of Etn (Fig. 3Bb, C).
364 Therefore, macroautophagic body was not observed in the vacuolar lumen of the starved
365 *cho1*Δ mutant both in the absence and presence of Etn (Figs. 2C and 3D).
366 Freeze-fracture EM has revealed that the vacuolar membrane exhibits characteristic
367 geometric patterns during the stationary phase [9, 10, 50], and that domains lacking the
368 transmembrane protein Vph1 correspond to raft-like regions [10, 51, 52]. In the present
369 study, freeze-fracture EM demonstrated that the vacuolar membrane of
370 the *cho1Δ* mutant exhibited such geometric patterns when starved in the presence, but
371 not in the absence, of Etn (Fig. 4A; Supplemental Fig. S6). Notably, invaginated,
372 intramembrane particle (IMP)-deficient raft-like domains, tightly associated with lipid
373 droplets (LDs; indicated by white double arrowheads in Fig. 4B), were observed under
374 these conditions. Furthermore, the IMP-rich, non-raft-like regions were confined to the
375 periphery of these raft-like protrusions, forming a distinct ring-like structure at the neck
376 of the balloon-shaped domain in the vacuolar membrane (arrows in Fig. S8; [10]).
377 Clusters of IMPs were also identified within vesicles in the vacuolar lumen (arrows in
378 Fig. S8), suggesting that these raft-like protrusions are severed at the non-raft regions,
379 completing the process of microautophagic lipophagy (Supplementary Fig. S3).
380 Previous studies have shown that PtdIns(3)P [10] and PtdIns(4)P [9] localize
381 specifically to the PF, but not the EF, of microautophagic vesicles in the vacuole. In
382 agreement with this, we found that in *cho1Δ* mutants starved in the presence of Etn,

383 both PtdIns(3)P (Fig. 2D) and PtdIns(4)P (Supplementary Fig. S9) were predominantly
384 localized to the PF of vesicles within the vacuole. Notably, the labeling density of
385 PtdIns(3)P on the PF of these vesicles was markedly reduced in *cho1Δ* cells compared
386 to WT [10, 14] and *psd1Δ/psd2Δ* mutants (Fig. 2A, B, D; Supplementary Fig. S2). A
387 similar reduction in PtdIns(3)P labeling was observed in the vacuolar membrane itself:
388 while PtdIns(3)P was consistently localized to the PF in WT cells [34], its density was
389 significantly lower in *cho1Δ* mutants (Fig. 4C; Supplementary Fig. S10). These findings
390 indicate that the vesicles present in the vacuolar lumen originate from the vacuolar
391 membrane and are microautophagic in nature (Supplementary Figs. S3, S8, and S11).
392 Consistently, using the QF-FRL method, we detected several microautophagic vesicles
393 in the vacuolar lumen of *cho1Δ* mutants starved in the presence, but not the absence, of
394 Etn (Fig. 5B). Vps27, a core component of the ESCRT-0 complex, is essential for
395 endosomal sorting [53] and has also been implicated in vacuolar microautophagic
396 lipophagy [54, 55]. In our study, no microautophagic vesicles were detected in the
397 vacuoles of *vps27Δ/cho1Δ* mutants, even when starved in the presence of Etn (Fig.
398 5Ad). Furthermore, the proportion of vacuolar membranes displaying geometric
399 patterns was drastically reduced in *vps27Δ/cho1Δ* mutants under these conditions (Fig.
400 6B, C). Collectively, these results suggest that microautophagic lipophagy is specifically
401 induced in *cho1Δ* mutants only when ethanolamine is present during starvation.
402

403 ***3. 3. Ubiquitin-conjugating E2 enzyme Ubc4 is required for microautophagic***
404 ***lipophagy***

405 Sakamaki et al. [56] recently reported that ubiquitin is conjugated to phospholipids,
406 mainly PtdEtn, in yeast and mammalian cells and showed that ubiquitinated PtdEtn

407 accumulates in the endosome and vacuole/lysosome membranes. Furthermore, they
408 reported that PtdEtn ubiquitination is facilitated by starvation in yeast cells [56]. In this
409 study, exogenously supplied Etn induced microautophagic lipophagy in the starved
410 *cho1*Δ mutant (Figs. 4 and 5), indicating that PtdEtn ubiquitination plays a role in
411 microautophagic lipophagy in the starved *cho1*Δ mutant. PtdEtn ubiquitination is
412 significantly reduced in the ubiquitin-conjugating enzyme (E2) gene *ubc4*-knocked-out
413 yeast [56]. Geometrical pattern of the vacuolar membrane, which was detected in the
414 *cho1*Δ mutant starved in the presence of Etn, was not observed in the starved
415 *ubc4*Δ/*cho1*Δ mutant in the presence of Etn (Fig. 6A, C). Furthermore, number of
416 microautophagic vesicles was drastically reduced in the vacuole of the *ubc4*Δ/*cho1*Δ
417 mutant starved in the presence of Etn (Fig. 5Ab, B). These findings emphasize the
418 essential role of the ubiquitin-conjugating E2 enzyme Ubc4 in microautophagic
419 lipophagy.

420 Our group and others [9, 10, 57] have reported that microautophagic lipophagy
421 of the vacuole occurs in acutely starved WT yeast, accompanied by the formation of
422 IMP-deficient raft-like domains in the vacuolar membrane. Microautophagic vesicles
423 were observed in the vacuoles of both WT and *psd1*Δ/*psd2*Δ mutants starved in S(-NC)
424 medium supplemented with PMSF, regardless of the presence or absence of Etn (Fig.
425 2A, B; Supplementally Fig. S2). Unexpectedly, microautophagic vesicles were also
426 detected in the vacuole of the starved *ubc4*Δ mutant (Fig. 5Ac). Furthermore, in acutely
427 starved WT yeast [10] and *ubc4*Δ mutant (Supplementally Fig. S12), raft-like domains
428 were restricted to specific regions of the vacuolar membrane, whereas in the stationary
429 phase [9, 10] and in the starved *cho1*Δ mutant supplemented with Etn (Fig. 4), the
430 vacuole was almost entirely covered with these domains. These findings suggest that

431 Ubc4 is not essential for vacuolar microautophagic lipophagy under acute starvation

432 conditions in WT yeast cells.

433 **4. Discussion**

434 In this study, we mainly found that (i) macroautophagy was defective in the
435 *cho1*Δ mutant, (ii) autophagosome was absent in the starved *cho1*Δ mutant, (iii)
436 microautophagic lipophagy was induced in the *cho1*Δ mutant starved in the presence of
437 Etn, and (iv) microautophagic lipophagy was inhibited in the starved *ubc4*Δ/*cho1*Δ
438 mutant in the presence of Etn.

439

440 ***4-1. Essential roles of PtdSer synthesized by Cho1p in the autophagosome formation***

441 In our previous study [15], we demonstrated the significant reduction in the
442 number of autophagosomes in the *osh5*Δ mutant compared to that in the WT strain,
443 suggesting the critical role of Osh5 in autophagosome formation. Additionally, we
444 reported thin inner and outer membranes of the autophagosome, if any, in the *osh5*Δ
445 mutant, along with low PtdSer labeling on the autophagosome membrane, emphasizing
446 the significance of PtdSer localization in autophagosome biogenesis [15]. Based on
447 these findings, we investigated the macroautophagic activity of the *cho1*Δ mutant using
448 the GFP-Atg8 processing assay in this study. We observed a significant defect in the
449 macroautophagic activity of the *cho1*Δ mutant, as evidenced by the absence of
450 autophagosomes in the cytoplasm following starvation, regardless of the presence or
451 absence of Etn (Fig. 1). These findings underscore the essential role of the PtdSer
452 synthase, Cho1, in autophagosome biogenesis.

453 In yeast cells, PtdEtn is synthesized via main two distinct pathways
454 (Supplementary Fig. S5). In one pathway, PtdEtn is produced from PtdSer by the
455 decarboxylases, Psd1 [44, 45] and Psd2 [46]. In the other pathway, PtdEtn is
456 synthesized via the Kennedy pathway using Etn and diacylglycerol [47, 58]. A previous

457 report suggested that PtdEtn is rarely formed in the *cho1*Δ mutant yeast in the absence
458 of Etn [59], in spite of the existence of other minor synthetic pathways of PtdEtn [48]
459 (Supplementary Fig. S5). Consistently, growth defects have been reported in the *cho1*Δ
460 mutant in the absence of Etn [59, 60]. PtdEtn is crucial for macroautophagy as its
461 conjugation with Atg8 is an essential step in autophagosome formation [42, 61]. In this
462 study, we observed significant macroautophagic activity, and autophagosomes in the
463 cytoplasm and many macroautophagic bodies in the vacuoles of WT yeast even in the
464 absence of Etn and *psd1*Δ/*psd2*Δ mutant in the presence or absence of Etn (Fig. 1).
465 These results were well consistent with the previous report in which the
466 macroautophagic activities were not inhibited in the *psd1*Δ or *psd2*Δ mutants [49].
467 These findings suggest that PtdEtn synthesized through both major and minor pathways
468 (Supplementary Fig. S5) contributes to yeast macroautophagy. In contrast to
469 macroautophagy, previous studies have shown that Psd1, but not Psd2, is essential for
470 mitochondria-specific autophagy (mitophagy) in yeast under acute nitrogen starvation
471 [49]. This indicates that PtdEtn, produced from PtdSer by the Psd1 decarboxylase
472 localized in the mitochondrial inner membrane [45], plays a crucial role in mitophagy
473 by facilitating Atg8 conjugation for autophagosome formation. In this study, we found
474 that macroautophagic activity was mostly inhibited, and no autophagosomes in the
475 cytoplasm or macroautophagic bodies in the vacuoles were observed in the starved
476 *cho1*Δ mutant, even in the presence of Etn (Figs. 1 and 3). These results indicate that
477 autophagosome formation does not occur even in the presence of PtdEtn, when PtdSer
478 is not synthesized using Cho1. To the best of our knowledge, this is the first study to
479 show that PtdSer synthesized using Cho1 is essential for autophagosome formation in
480 yeast cells. However, further studies are necessary to elucidate the action mechanisms

481 of PtdSer in autophagosome formation.

482

483 ***4-2. Inducible microautophagic lipophagy in the starved cho1Δ mutant***

484 Here, microautophagic lipophagy was induced in the starved *cho1*Δ mutant
485 yeast when Etn was exogenously added to the medium. This indicates the important role
486 of exogenous Etn in microautophagic lipophagy. As described above, two major
487 pathways (Supplementary Fig. S5), one involving the conversion of PtdSer by Psd1 [44,
488 45] or Psd2 [46] and the other involving the Kennedy pathway [47], are involved in
489 PtdEtn synthesis; however, additional minor pathways may also exist in yeast cells [48].
490 Yeast cells with mutations in *cho1* gene require exogenous Etn for normal growth [59].
491 In this study, we added Etn to the medium to culture the *cho1*Δ mutant as its growth was
492 extremely slow in the absence of Etn (see the Methods section), similar to previous
493 reports [59, 60]. *cho1* mutants exhibit low levels of PtdEtn in the absence of Etn but
494 normal levels of PtdEtn in the presence of Etn [59]. Therefore, exogenously supplied
495 Etn facilitates the synthesis of PtdEtn in the *cho1*Δ mutant, and the synthesized PtdEtn
496 is essential for the induction of microautophagic lipophagy under starved conditions.
497 Additionally, Vps27 is the central factor of the ESCRT-0 complex in yeast cells [53] and
498 we observed almost no microautophagic vesicles in the vacuoles of the *vps27*Δ/*cho1*Δ
499 mutant starved in the presence of Etn (Fig. 5Ad). These results are consistent with a
500 previous report [54, 55] that microautophagic lipophagy, which is induced after a
501 diauxic shift or a starvation, is abolished in the *vps27* gene-deletion mutant. Here,
502 microautophagic lipophagy was induced in the starved *cho1*Δ mutant in the presence,
503 but not in absence, of Etn. To the best of our knowledge, this is the first study to show
504 that PtdEtn, synthesized via the Kennedy pathway, plays a crucial role in

505 microautophagic lipophagy.

506

507 ***4-3. Crucial roles of ubiquitin-conjugating E2 enzyme Ubc4 for microautophagic***

508 ***lipophagy***

509 Sakamaki et al. [56] used a biochemical technique and reported that

510 ubiquitinated PtdEtn is localized in the endosome- or vacuole/lysosome-rich membrane

511 fractions, suggesting its localization in the membranes of endosomes and

512 vacuoles/lysosomes. They also showed PtdEtn ubiquitination in the endosomal and

513 vacuolar membranes is facilitated by starvation [56]. In yeast cells, PtdEtn

514 ubiquitination is catalyzed by the ubiquitin-activating enzyme (E1), Uba1, ubiquitin-

515 conjugating enzymes (E2s), Ubc4 and Ubc5, and ubiquitin ligase (E3), Tul1 [56]. In this

516 study, we found that the microautophagic lipophagy was defective in the starved

517 *ubc4*Δ/*cho1*Δ mutant in the presence of Etn (Figs. 5 and 6). PtdEtn ubiquitination is

518 strongly suppressed in the *ubc4*Δ mutant [56]. These results suggest that PtdEtn

519 ubiquitination plays a crucial role in microautophagic lipophagy in yeast cells.

520 Liposomes containing ubiquitinated PtdEtn specifically recruit the ESCRT components,

521 Vps27-Hse-1 (ESCRT-0) and Vps23 (a component of ESCRT-1), in vitro [56].

522 Consistently, in this study, no microautophagic vesicles were observed in the vacuoles

523 of the starved *vps27*Δ/*cho1*Δ mutant in the presence of Etn (Fig. 5Ad).

524 In this study, PtdEtn was localized in the PF, but not the EF, leaflets of the

525 vacuolar membrane, which exhibited a geometrical pattern in the starved *cho1*Δ mutant

526 in the presence of Etn (Supplementary Fig. S13). Conversely, PtdEtn was localized to

527 both the PF and EF of the vacuolar membrane and exhibited a normal round pattern in

528 starved WT yeast. PtdEtn labeling density in EF, but not in PF, of the vacuolar

529 membrane with the geometric pattern in the starved *cho1*Δ mutant was significantly
530 lower than that in starved WT yeast (Supplementary Fig. S13B). Although whether the
531 PtdEtn-specific binding probe, duramycin, binds to ubiquitinated PtdEtn remains
532 unclear, PtdEtn localized in the cytoplasmic leaflet of the vacuolar membrane is readily
533 ubiquitinated. The ubiquitinated PtdEtn localized in the cytoplasmic leaflet further
534 recruits the ESCRT components, Vps27-Hse1 and Vps23 [56]. Here, vacuolar
535 membranes with geometric patterns were mostly absent in the *ubc4*Δ/*cho1*Δ and
536 *vps27*Δ/*cho1*Δ mutants starved in the presence of Etn (Fig. 6). Formation of an IMP-
537 deficient raft-like domain in the vacuolar membrane with geometric pattern is crucial
538 for the invagination of LDs into the vacuolar lumen, facilitating microautophagic
539 lipophagy [9, 10] (Supplementary Fig. S8). These findings suggest that the binding of
540 Vps27 to ubiquitinated PtdEtn is essential for the formation of an IMP-deficient raft-
541 like domain in the vacuolar membrane exhibiting a geometric pattern. Ubiquitinated
542 PtdEtn on vacuoles is recognized by various ESCRT components, including Vps23 and
543 Hse1, ultimately leading to the recruitment of downstream ESCRT components and
544 inward membrane invagination [62]. However, the ubiquitin-conjugating E2 enzyme
545 Ubc4 can ubiquitinate not only PtdEtn but also various other substrates [63]. Indeed,
546 Vps27, which contains ubiquitin-interacting motifs (UIMs), has been reported to bind
547 ubiquitinated proteins at the endosome [64, 65]. Furthermore, we did not directly assess
548 the ubiquitination level of PtdEtn under our experimental conditions. Therefore, we
549 cannot rule out the possibility that Ubc4-mediated ubiquitination of molecules other
550 than PtdEtn contributes to the microautophagic lipophagy of vacuoles in the starved
551 *cho1*Δ mutant in the presence of Etn. Further investigations are required to clarify the
552 precise mechanisms by which ubiquitinated PtdEtn induces microautophagic lipophagy.

553 In this study, we demonstrated that microautophagic vesicles were present in
554 the vacuole of acutely starved WT yeast and the *psd1*Δ/*psd2*Δ mutant, regardless of the
555 presence of Etn (Fig. 2). These findings align well with previous reports from our group
556 and others [9, 10, 57]. However, while microautophagic lipophagy was observed in the
557 acutely starved *cho1*Δ mutant with Etn, it was inhibited in the *ubc4*-deletion mutant
558 (*ubc4*Δ/*cho1*Δ, Fig. 5), despite remaining intact in the starved *ubc4*Δ mutant (Fig. 5).
559 Additionally, we observed that IMP-deficient raft-like domains were partially present in
560 the vacuolar membrane of acutely starved WT yeast [9, 10] and *ubc4*Δ mutant
561 (Supplementary Fig. S12). In contrast, these domains entirely covered the vacuolar
562 membrane in the starved *cho1*Δ mutant with Etn (Fig. 4, Supplementary Fig. S8) [9, 10].
563 These results suggest that the mechanisms underlying microautophagic lipophagy may
564 differ depending on whether microautophagic lipophagy is associated with the geometric
565 pattern of IMP-deficient raft-like domains. Further investigations will be necessary to
566 elucidate the precise mechanisms governing microautophagic lipophagy.
567
568 ***4-4. Formation of IMP-deficient raft-like domain in the vacuolar membrane and***
569 ***microautophagic lipophagy***
570 It has been reported that IMP-deficient raft-like domains in the vacuolar membrane play
571 critical roles in microautophagic lipophagy during both stationary phase and acute
572 starvation [9, 10, 52]. Cholesterol transport to the vacuolar membrane via Niemann-
573 Pick type C (NPC) proteins—NPC1 and NPC2 (Ncr1 and Npc2 in yeast,
574 respectively)—is essential for the expansion of these IMP-deficient raft-like domains
575 [10]. In mammalian cells, intraluminal vesicles (ILVs) within multivesicular bodies
576 (MVBs) have been shown to be enriched in sterols [66]. Furthermore, ILVs are

577 frequently observed in the vacuoles of acutely starved *ncr1*Δ/*npc2*Δ mutants and in
578 mutants lacking the major vacuolar proteases Pep4 and Prb1 [10]. Notably, the
579 formation of IMP-deficient raft-like domains and microautophagic lipophagy during
580 stationary phase is absent in *vps4*Δ mutants, in which the MVB pathway is disrupted
581 [10]. In line with these findings, we also observed pronounced accumulation of ILVs
582 and autophagic bodies within the vacuolar lumen of starved *pep4*Δ mutants
583 (Supplemental Fig. S14), whereas such structures were only rarely found in WT yeasts.
584 These observations support the idea that ILVs within MVBs represent a major sterol
585 source for NPC-mediated expansion of IMP-deficient raft-like domains in the yeast
586 vacuolar membrane [10]. In the present study, we further demonstrated that both IMP-
587 deficient raft-like domain formation (Fig. 6) and microautophagic lipophagy (Fig. 5)
588 were largely abolished in starved *vps27*Δ/*cho1*Δ and *ubc4*Δ/*cho1*Δ mutants in the
589 presence of Etn. It is well established that Vps27 (ESCRT-0) is essential for the MVB
590 pathway in endosomes [62], and that PtdEtn ubiquitinated by Ubc4 can recruit Vps27 to
591 the endosomal membrane [56]. We therefore hypothesize that blocking sterol transport
592 from the MVB to the vacuolar membrane leads to the loss of IMP-deficient raft-like
593 domain formation and microautophagic lipophagy in starved *vps27*Δ/*cho1*Δ and
594 *ubc4*Δ/*cho1*Δ mutants, indicating an indirect role for Vps27 and Ubc4 in these
595 processes.
596 Additionally, it was shown that raft-like domain formation and
597 microautophagic lipophagy were only partially diminished in *are1*Δ/*are2*Δ mutants,
598 which are defective in sterol ester synthesis (see Figure 6-figure supplement 2 in [10]),
599 suggesting that mechanisms other than cholesterol transport also contribute to the
600 expansion of IMP-deficient raft-like domains in the yeast vacuolar membrane. We

601 further propose that ubiquitination of specific molecules by Ubc4 may directly facilitate
602 the expansion of raft-like domains and promote microautophagic lipophagy in the yeast
603 vacuole. Further studies will be necessary to elucidate the molecular mechanisms
604 underlying the expansion of IMP-deficient raft-like domains in the vacuolar membrane
605 and the process of microautophagic lipophagy in yeast cells.
606

607 **References**

608 [1] N. Mizushima, M. Komatsu, Autophagy: renovation of cells and tissues, Cell, 147
609 (2011) 728-741.
610 [2] Z. Xie, D.J. Klionsky, Autophagosome formation: core machinery and adaptations,
611 Nat Cell Biol, 9 (2007) 1102-1109.
612 [3] D. Mijaljica, M. Prescott, R.J. Devenish, Microautophagy in mammalian cells:
613 revisiting a 40-year-old conundrum, Autophagy, 7 (2011) 673-682.
614 [4] C. De Duve, R. Wattiaux, Functions of lysosomes, Annu Rev Physiol, 28 (1966)
615 435-492.
616 [5] D.L. Tuttle, W.A. Dunn, Jr., Divergent modes of autophagy in the methylotrophic
617 yeast Pichia pastoris, J Cell Sci, 108 (Pt 1) (1995) 25-35.
618 [6] T. Osawa, T. Kotani, T. Kawaoka, E. Hirata, K. Suzuki, H. Nakatogawa, Y. Ohsumi,
619 N.N. Noda, Atg2 mediates direct lipid transfer between membranes for
620 autophagosome formation, Nat Struct Mol Biol, 26 (2019) 281-288.
621 [7] S. Maeda, H. Yamamoto, L.N. Kinch, C.M. Garza, S. Takahashi, C. Otomo, N.V.
622 Grishin, S. Forli, N. Mizushima, T. Otomo, Structure, lipid scrambling activity and
623 role in autophagosome formation of ATG9A, Nat Struct Mol Biol, 27 (2020) 1194-
624 1201.
625 [8] K. Matoba, T. Kotani, A. Tsutsumi, T. Tsuji, T. Mori, D. Noshiro, Y. Sugita, N.
626 Nomura, S. Iwata, Y. Ohsumi, T. Fujimoto, H. Nakatogawa, M. Kikkawa, N.N.
627 Noda, Atg9 is a lipid scramblase that mediates autophagosomal membrane
628 expansion, Nat Struct Mol Biol, 27 (2020) 1185-1193.
629 [9] Y. Kurokawa, R. Konishi, A. Yoshida, K. Tomioku, K. Tanabe, A. Fujita,
630 Microautophagy in the yeast vacuole depends on the activities of

631 phosphatidylinositol 4-kinases, Stt4p and Pik1p, Biochim Biophys Acta Biomembr,
632 1862 (2020) 183416.
633 [10] T. Tsuji, M. Fujimoto, T. Tatematsu, J. Cheng, M. Orii, S. Takatori, T. Fujimoto,
634 Niemann-Pick type C proteins promote microautophagy by expanding raft-like
635 membrane domains in the yeast vacuole, Elife, 6 (2017).
636 [11] S. Maeda, C. Otomo, T. Otomo, The autophagic membrane tether ATG2A transfers
637 lipids between membranes, Elife, 8 (2019).
638 [12] K. Tsuboyama, I. Koyama-Honda, Y. Sakamaki, M. Koike, H. Morishita, N.
639 Mizushima, The ATG conjugation systems are important for degradation of the
640 inner autophagosomal membrane, Science, 354 (2016) 1036-1041.
641 [13] Y. Kurokawa, A. Yoshida, E. Fujii, K. Tomioku, H. Hayashi, K. Tanabe, A. Fujita,
642 Phosphatidylinositol 4-phosphate on Rab7-positive autophagosomes revealed by
643 the freeze-fracture replica labeling, Traffic, 20 (2019) 82-95.
644 [14] Y. Yamakuchi, Y. Kurokawa, R. Konishi, K. Fukuda, T. Masatani, A. Fujita,
645 Selective increment of phosphatidylserine on the autophagic body membrane in the
646 yeast vacuole, FEBS Lett, 595 (2021) 2197-2207.
647 [15] M. Muramoto, N. Mineoka, K. Fukuda, S. Kuriyama, T. Masatani, A. Fujita,
648 Coordinated regulation of phosphatidylinositol 4-phosphate and phosphatidylserine
649 levels by Osh4p and Osh5p is an essential regulatory mechanism in autophagy,
650 Biochim Biophys Acta Biomembr, 1866 (2024) 184308.
651 [16] J.H. Hurley, T. Meyer, Subcellular targeting by membrane lipids, Curr Opin Cell
652 Biol, 13 (2001) 146-152.
653 [17] P. Varnai, T. Balla, Visualization of phosphoinositides that bind pleckstrin
654 homology domains: calcium- and agonist-induced dynamic changes and

655 relationship to myo-[3H]inositol-labeled phosphoinositide pools, J Cell Biol, 143
656 (1998) 501-510.
657 [18] H. Bisio, A. Krishnan, J.B. Marq, D. Soldati-Favre, Toxoplasma gondii
658 phosphatidylserine flippase complex ATP2B-CDC50.4 critically participates in
659 microneme exocytosis, PLoS Pathog, 18 (2022) e1010438.
660 [19] T.E. Rusten, H. Stenmark, Analyzing phosphoinositides and their interacting
661 proteins, Nat Methods, 3 (2006) 251-258.
662 [20] G.R. Hammond, T. Balla, Polyphosphoinositide binding domains: Key to inositol
663 lipid biology, Biochim Biophys Acta, 1851 (2015) 746-758.
664 [21] O.V. Vieira, R.E. Harrison, C.C. Scott, H. Stenmark, D. Alexander, J. Liu, J.
665 Gruenberg, A.D. Schreiber, S. Grinstein, Acquisition of Hrs, an essential
666 component of phagosomal maturation, is impaired by mycobacteria, Mol Cell Biol,
667 24 (2004) 4593-4604.
668 [22] S.A. Watt, G. Kular, I.N. Fleming, C.P. Downes, J.M. Lucocq, Subcellular
669 localization of phosphatidylinositol 4,5-bisphosphate using the pleckstrin homology
670 domain of phospholipase C delta1, Biochem J, 363 (2002) 657-666.
671 [23] J. van Rheenen, E.M. Achame, H. Janssen, J. Calafat, K. Jalink, PIP2 signaling in
672 lipid domains: a critical re-evaluation, EMBO J, 24 (2005) 1664-1673.
673 [24] G.D. Fairn, N.L. Schieber, N. Ariotti, S. Murphy, L. Kuerschner, R.I. Webb, S.
674 Grinstein, R.G. Parton, High-resolution mapping reveals topologically distinct
675 cellular pools of phosphatidylserine, J Cell Biol, 194 (2011) 257-275.
676 [25] A. Fujita, J. Cheng, T. Fujimoto, Quantitative electron microscopy for the
677 nanoscale analysis of membrane lipid distribution, Nat Protoc, 5 (2010) 661-669.
678 [26] A. Fujita, J. Cheng, M. Hirakawa, K. Furukawa, S. Kusunoki, T. Fujimoto,

679 Gangliosides GM1 and GM3 in the living cell membrane form clusters susceptible
680 to cholesterol depletion and chilling, Mol Biol Cell, 18 (2007) 2112-2122.
681 [27] A. Fujita, J. Cheng, K. Tauchi-Sato, T. Takenawa, T. Fujimoto, A distinct pool of
682 phosphatidylinositol 4,5-bisphosphate in caveolae revealed by a nanoscale labeling
683 technique, Proc Natl Acad Sci U S A, 106 (2009) 9256-9261.
684 [28] A. Yoshida, M. Shigekuni, K. Tanabe, A. Fujita, Nanoscale analysis reveals
685 agonist-sensitive and heterogeneous pools of phosphatidylinositol 4-phosphate in
686 the plasma membrane, Biochim Biophys Acta, 1858 (2016) 1298-1305.
687 [29] J.S. Robinson, D.J. Klionsky, L.M. Banta, S.D. Emr, Protein sorting in
688 Saccharomyces cerevisiae: isolation of mutants defective in the delivery and
689 processing of multiple vacuolar hydrolases, Mol Cell Biol, 8 (1988) 4936-4948.
690 [30] U. Guldener, S. Heck, T. Fielder, J. Beinhauer, J.H. Hegemann, A new efficient
691 gene disruption cassette for repeated use in budding yeast, Nucleic Acids Res, 24
692 (1996) 2519-2524.
693 [31] K. Suzuki, T. Kirisako, Y. Kamada, N. Mizushima, T. Noda, Y. Ohsumi, The pre-
694 autophagosomal structure organized by concerted functions of APG genes is
695 essential for autophagosome formation, EMBO J, 20 (2001) 5971-5981.
696 [32] H. Cheong, D.J. Klionsky, Biochemical methods to monitor autophagy-related
697 processes in yeast, Methods Enzymol, 451 (2008) 1-26.
698 [33] T. Fujimoto, K. Fujimoto, Metal sandwich method to quick-freeze monolayer
699 cultured cells for freeze-fracture, J Histochem Cytochem, 45 (1997) 595-598.
700 [34] J. Cheng, A. Fujita, H. Yamamoto, T. Tatematsu, S. Kakuta, K. Obara, Y. Ohsumi,
701 T. Fujimoto, Yeast and mammalian autophagosomes exhibit distinct
702 phosphatidylinositol 3-phosphate asymmetries, Nat Commun, 5 (2014) 3207.

703 [35] K. Obara, T. Noda, K. Niimi, Y. Ohsumi, Transport of phosphatidylinositol 3-
704 phosphate into the vacuole via autophagic membranes in Saccharomyces cerevisiae,
705 Genes Cells, 13 (2008) 537-547.
706 [36] Y. Kurokawa, R. Konishi, A. Yoshida, K. Tomioku, T. Futagami, H. Tamaki, K.
707 Tanabe, A. Fujita, Essential and distinct roles of phosphatidylinositol 4-kinases,
708 Pik1p and Stt4p, in yeast autophagy, Biochim Biophys Acta Mol Cell Biol Lipids,
709 1864 (2019) 1214-1225.
710 [37] M. Baba, M. Osumi, Y. Ohsumi, Analysis of the membrane structures involved in
711 autophagy in yeast by freeze-replica method, Cell Struct Funct, 20 (1995) 465-471.
712 [38] A. Adachi, M. Koizumi, Y. Ohsumi, Autophagy induction under carbon starvation
713 conditions is negatively regulated by carbon catabolite repression, J Biol Chem,
714 292 (2017) 19905-19918.
715 [39] T. Nishimura, N. Tamura, N. Kono, Y. Shimanaka, H. Arai, H. Yamamoto, N.
716 Mizushima, Autophagosome formation is initiated at phosphatidylinositol synthase-
717 enriched ER subdomains, EMBO J, 36 (2017) 1719-1735.
718 [40] A. Kihara, T. Noda, N. Ishihara, Y. Ohsumi, Two distinct Vps34
719 phosphatidylinositol 3-kinase complexes function in autophagy and
720 carboxypeptidase Y sorting in Saccharomyces cerevisiae, J Cell Biol, 152 (2001)
721 519-530.
722 [41] K. Wang, Z. Yang, X. Liu, K. Mao, U. Nair, D.J. Klionsky, Phosphatidylinositol 4-
723 kinases are required for autophagic membrane trafficking, J Biol Chem, 287 (2012)
724 37964-37972.
725 [42] Y. Ichimura, T. Kirisako, T. Takao, Y. Satomi, Y. Shimonishi, N. Ishihara, N.
726 Mizushima, I. Tanida, E. Kominami, M. Ohsumi, T. Noda, Y. Ohsumi, A ubiquitin-

727 like system mediates protein lipidation, Nature, 408 (2000) 488-492.
728 [43] Y. Kabeya, N. Mizushima, T. Ueno, A. Yamamoto, T. Kirisako, T. Noda, E.
729 Kominami, Y. Ohsumi, T. Yoshimori, LC3, a mammalian homologue of yeast
730 Apg8p, is localized in autophagosome membranes after processing, EMBO J, 19
731 (2000) 5720-5728.
732 [44] C.J. Clancey, S.C. Chang, W. Dowhan, Cloning of a gene (PSD1) encoding
733 phosphatidylserine decarboxylase from Saccharomyces cerevisiae by
734 complementation of an Escherichia coli mutant, J Biol Chem, 268 (1993) 24580-
735 24590.
736 [45] P.J. Trotter, J. Pedretti, D.R. Voelker, Phosphatidylserine decarboxylase from
737 Saccharomyces cerevisiae. Isolation of mutants, cloning of the gene, and creation of
738 a null allele, J Biol Chem, 268 (1993) 21416-21424.
739 [46] P.J. Trotter, J. Pedretti, R. Yates, D.R. Voelker, Phosphatidylserine decarboxylase 2
740 of Saccharomyces cerevisiae. Cloning and mapping of the gene, heterologous
741 expression, and creation of the null allele, J Biol Chem, 270 (1995) 6071-6080.
742 [47] S.A. Henry, S.D. Kohlwein, G.M. Carman, Metabolism and regulation of
743 glycerolipids in the yeast Saccharomyces cerevisiae, Genetics, 190 (2012) 317-349.
744 [48] E. Calzada, O. Onguka, S.M. Claypool, Phosphatidylethanolamine Metabolism in
745 Health and Disease, Int Rev Cell Mol Biol, 321 (2016) 29-88.
746 [49] P. Vigie, E. Cougouilles, I. Bhatia-Kissova, B. Salin, C. Blancard, N. Camougrand,
747 The mitochondrial phosphatidylserine decarboxylase Psd1 is involved in nitrogen
748 starvation-induced mitophagy in yeast, J Cell Sci, 132 (2019).
749 [50] C.H. Moeller, W.W. Thomson, An ultrastructural study of the yeast tomoplast
750 during the shift from exponential to stationary phase, J Ultrastruct Res, 68 (1979)

751 28-37.
752 [51] A. Toulmay, W.A. Prinz, Direct imaging reveals stable, micrometer-scale lipid
753 domains that segregate proteins in live cells, J Cell Biol, 202 (2013) 35-44.
754 [52] C.W. Wang, Y.H. Miao, Y.S. Chang, A sterol-enriched vacuolar microdomain
755 mediates stationary phase lipophagy in budding yeast, J Cell Biol, 206 (2014) 357-
756 366.
757 [53] R.C. Piper, A.A. Cooper, H. Yang, T.H. Stevens, VPS27 controls vacuolar and
758 endocytic traffic through a prevacuolar compartment in Saccharomyces cerevisiae,
759 J Cell Biol, 131 (1995) 603-617.
760 [54] M. Oku, Y. Maeda, Y. Kagohashi, T. Kondo, M. Yamada, T. Fujimoto, Y. Sakai,
761 Evidence for ESCRT- and clathrin-dependent microautophagy, J Cell Biol, 216
762 (2017) 3263-3274.
763 [55] S. Morshed, M.N. Tasnin, T. Ushimaru, ESCRT machinery plays a role in
764 microautophagy in yeast, BMC Mol Cell Biol, 21 (2020) 70.
765 [56] J.I. Sakamaki, K.L. Ode, Y. Kurikawa, H.R. Ueda, H. Yamamoto, N. Mizushima,
766 Ubiquitination of phosphatidylethanolamine in organellar membranes, Mol Cell, 82
767 (2022) 3677-3692 e3611.
768 [57] T. van Zutphen, V. Todde, R. de Boer, M. Kreim, H.F. Hofbauer, H. Wolinski, M.
769 Veenhuis, I.J. van der Klei, S.D. Kohlwein, Lipid droplet autophagy in the yeast
770 Saccharomyces cerevisiae, Mol Biol Cell, 25 (2014) 290-301.
771 [58] G.M. Carman, G.S. Han, Regulation of phospholipid synthesis in the yeast
772 Saccharomyces cerevisiae, Annu Rev Biochem, 80 (2011) 859-883.
773 [59] K.D. Atkinson, B. Jensen, A.I. Kolat, E.M. Storm, S.A. Henry, S. Fogel, Yeast
774 mutants auxotrophic for choline or ethanolamine, J Bacteriol, 141 (1980) 558-564.

775 [60] J.I. Nikawa, S. Yamashita, Characterization of phosphatidylserine synthase from
776 Saccharomyces cerevisiae and a mutant defective in the enzyme, Biochim Biophys
777 Acta, 665 (1981) 420-426.
778 [61] Y. Kabeya, N. Mizushima, A. Yamamoto, S. Oshitani-Okamoto, Y. Ohsumi, T.
779 Yoshimori, LC3, GABARAP and GATE16 localize to autophagosomal membrane
780 depending on form-II formation, J Cell Sci, 117 (2004) 2805-2812.
781 [62] W.M. Henne, N.J. Buchkovich, S.D. Emr, The ESCRT pathway, Dev Cell, 21
782 (2011) 77-91.
783 [63] W. Seufert, S. Jentsch, Ubiquitin-conjugating enzymes UBC4 and UBC5 mediate
784 selective degradation of short-lived and abnormal proteins, EMBO J, 9 (1990) 543-
785 550.
786 [64] S.C. Shih, D.J. Katzmann, J.D. Schnell, M. Sutanto, S.D. Emr, L. Hicke, Epsins
787 and Vps27p/Hrs contain ubiquitin-binding domains that function in receptor
788 endocytosis, Nat Cell Biol, 4 (2002) 389-393.
789 [65] P.S. Bilodeau, J.L. Urbanowski, S.C. Winistorfer, R.C. Piper, The Vps27p Hse1p
790 complex binds ubiquitin and mediates endosomal protein sorting, Nat Cell Biol, 4
791 (2002) 534-539.
792 [66] W. Mobius, Y. Ohno-Iwashita, E.G. van Donselaar, V.M. Oorschot, Y. Shimada, T.
793 Fujimoto, H.F. Heijnen, H.J. Geuze, J.W. Slot, Immunoelectron microscopic
794 localization of cholesterol using biotinylated and non-cytolytic perfringolysin O, J
795 Histochem Cytochem, 50 (2002) 43-55.

Acknowledgments

We would like to thank Dr. Toyoshi Fujimoto (Juntendo University) for kindly gifting the wild-type yeast (SEY6210) and Editage (www.editage.com) for English language editing.

Funding

This study was supported by JSPS KAKENHI [grant no. JP25K09420, JP22K19252, JP20H03154], research grants from the Ito Foundation, the Nakatani Foundation for Advancement of Measuring Technologies in Biomedical Engineering, Takeda Science Foundation, Naito Foundation, ONO Medical Research Foundation, NOVARTIS Foundation (Japan) for the Promotion of Science, and the Uehara Memorial Foundation (to A.F.). The funding sources were not involved in the study design; collection, analysis, and interpretation of data; writing of the report; or decision to submit the article for publication.

Author contributions

All authors contributed to the conception and design of this study. N. M., R. K., M. M., K. F., S. K., T. M., and A. F. performed material preparation, data collection, and analysis. A. F. wrote the first draft of the manuscript, and all authors commented on the previous versions of the manuscript. All the authors have read and approved the final version of the manuscript.

Data availability

All data generated or analyzed during this study are included in this published article (and its Supplementary information files).

Competing interests

The authors declare no potential conflicts of interest.

824 **Figure legends**

825 **Figure 1. Defects in autophagosome formation and autophagic activity in *cho1*Δ**
826 **yeast.**

827 (A) Autophagosomes in wild-type (WT) cultured in S(-NC) for 5 hr. The
828 autophagosome was identified as s smooth-surfaced double-membrane structure, and
829 seen in two different patterns, as shown in the diagrams in (c). (a) Convex structure
830 displaying the outer membrane (OM) EF (yellow line, $_{E}$OM) and the inner membrane
831 (IM) PF (blue line, $_{P}$IM). (b) Concave structure displaying the OM PF (red line, $_{P}$OM)
832 and the IM EF (green line, $_{E}$IM). The labelings of PtdIns(3)P were detected in the EF of
833 both the outer (a) and inner (b) autophagosome membranes. Scale bar, 200 nm. (B) WT
834 yeast cultured in S(-NC) supplemented with PMSF for 5 h. PtdIns(3)P was labelled
835 intensely in the EF (green) of macroautophagic body membranes in the vacuolar lumen.
836 A lower amount of labelling was also seen in the PF (blue) of macroautophagic body
837 membranes. Double arrowheads, vacuole. Scale bar, 500 nm. (C) The freeze-fracture
838 EM showed that autophagosomes were observed in the cytosol of WT, *psd1*Δ/*psd2*Δ,
839 and *ubc4*Δ strains after incubation in S(-NC) for 5 h. However, almost no
840 autophagosomes were detected in the cytosol of *cho1*Δ mutant strain in both the
841 presence and absence of Etn in the S(-NC) medium. Mean ± standard error (SE) of three
842 independent experiments (>35 cells were counted in each group in each experiment).
843 The number of autophagosomes per cell in each strain was compared to that in WT
844 yeast. Dunnett's test: n.s., not significant; *$p < 0.05$. (D) Green fluorescent protein
845 (GFP)-autophagy-related gene (Atg)-8 degradation via macroautophagy in the *cho1*Δ
846 mutant. Wild-type (WT), *psd1*Δ/*psd2*Δ, and *cho1*Δ strains transformed with a plasmid
847 expressing GFP-Atg8 under the control of the *CUP1* promoter were grown in SMD-Ura

848 medium at 30 °C in the presence or absence of 3 mM ethanolamine (Etn) to mid-log
849 phase. For each strain, the culture was divided into three aliquots. One aliquot was
850 cultured in YPD medium for 4 h at 30 °C. The other aliquots were shifted to S(-NC) and
851 cultured for 4 h at 30 °C in the presence or absence of Etn. For each aliquot, samples
852 were taken before (+NC) and after (-NC) starvation without PMSF. Bands of full-length
853 GFP-Atg8 and free GFP are shown. Defect in GFP-Atg8 degradation was observed in
854 the *cho1*Δ mutant in both the presence and absence of Etn.
855
856 **Figure 2. Phosphatidylinositol 3-phosphate (PtdIns(3)P) labeling of vesicle**
857 **membranes in the vacuoles of starved WT yeast, *psd1*Δ/*psd2*Δ, *cho1*Δ, and *ubc4*Δ**
858 **mutants.**
859 WT yeast (A), *psd1*Δ/*psd2*Δ (B), *cho1*Δ (C), and *ubc4*Δ mutant strains were starved in
860 S(-NC) medium supplemented with PMSF for 5 h at 30 °C, both in the absence (a) and
861 presence (b) of ethanolamine (Etn). In WT yeast (A), and the *psd1*Δ/*psd2*Δ (B) and
862 *ubc4*Δ mutants, two types of vesicles were observed under both conditions: one with
863 PtdIns(3)P labeling enriched in the external face (EF, green), but not cytoplasmic face
864 (PF, blue), of vesicles in the vacuoles and another with labeling in the peripheral face
865 (PF, orange), but not the EF (purple) (D, see also Supplementary Fig. S2). In contrast,
866 no vesicles were detected in the vacuoles of the *cho1*Δ mutant in the absence of Etn
867 (Ca). However, in the presence of Etn, numerous vesicles were observed in the vacuoles
868 of the *cho1*Δ mutant (Cb). Unlike WT yeast, and the *psd1*Δ/*psd2*Δ and *ubc4*Δ mutants,
869 only one type of vesicle was detected in the *cho1*Δ mutant with Etn supplementation. In
870 these vesicles, PtdIns(3)P labeling was localized to the PF (orange) but not the EF
871 (purple) of the vesicle membranes in the vacuoles (Cb, D). This characterization of the

872 PtdIns(3)P labelings indicates that these vesicles in the vacuole of the *cho1*Δ mutant
873 were microautophagic vesicles. The microautophagic vesicles were classified when the
874 labeling densities of PtdIns(3)P were more than 200 golds/μm^2 in the PF and less than
875 50 golds/μm^2 in the EF of vesicular membrane. Mean ± SE of three independent
876 experiments (>10 vacuoles were counted in each group in each experiment). PtdIns(3)P
877 labeling in the PF was compared with that in the EF. *t*-test: *** $p < 0.001$. Scale bar:
878 500 nm.
879
880 **Figure 3. PtdEtn labeling of autophagosome membrane, macroautophagic body,**
881 **and microautophagic vesicle in WT yeast, the *psd1*Δ/*psd2*Δ, *cho1*Δ, and *ubc4*Δ**
882 **mutants.**
883 WT, *psd1*Δ/*psd2*Δ, *cho1*Δ, and *ubc4*Δ yeast strains were starved in the S(-NC) medium
884 supplemented with PMSF in the absence and presence of Etn at 30 °C for 5 h.
885 Microphotographs of autophagosomes (A), macroautophagic bodies, and
886 microautophagic vesicles in the vacuoles of WT yeast (Ba) and the *cho1*Δ mutant (Bb)
887 are shown. PtdEtn labeling was detected in both the EF and PF of the inner and outer
888 membranes of autophagosomes (A) in the cytoplasm and macroautophagic bodies (Ba)
889 in vacuoles. In the *cho1*Δ mutant, PtdEtn labeling was localized in the PF, but not the
890 EF, in the membrane of the microautophagic vesicles in the vacuoles (Bb). Gold
891 labeling densities of EF were not significantly different from those of PF in the
892 membranes of macroautophagic bodies (C). IM: inner membrane, OM: outer
893 membrane. Mean ± SE of three independent experiments (>30 autophagosomes or
894 vesicles were counted in each group in each experiment). PtdEtn labeling in PF was
895 compared to that in EF. *t*-test; n.s., not significant; ***$p < 0.001$. (D) According to the

896 localization pattern of PtdIns(3)P (Fig. 2) and PtdEtn labeling in EF or PF of the
897 vesicular membranes, the numbers of the macroautophagic bodies in the vacuoles of
898 WT, *psd1*Δ/*psd2*Δ, *cho1*Δ, and *ubc4*Δ strains were determined. Several
899 macroautophagic bodies were detected in WT yeast and *psd1*Δ/*psd2*Δ in the presence
900 and absence of the Etn, but almost none were detected in the vacuoles of *cho1*Δ mutant
901 in both the presence and absence of Etn. Mean ± SE of three independent experiments
902 (>20 vacuoles were counted in each group in each experiment). The number of
903 macroautophagic bodies in the vacuoles of each strain was compared to that in WT
904 yeast in the absence of Etn. Dunnett's test: n.s., not significant; *$p < 0.05$.
905
906 **Figure 4. Microautophagic lipophagy in the starved *cho1*Δ mutant occurs via the**
907 **expansion of raft-like vacuolar membrane in the presence of Etn.**
908 *cho1*Δ mutant yeast was incubated in S(-NC) medium supplemented with PMSF in the
909 presence of Etn at 30 °C for 5 h. Freeze-fracture EM method and PtdIns(3)P labeling of
910 the vacuolar membrane (A and B). Vacuolar membrane in *cho1*Δ mutant starved in the
911 presence of the Etn showed geometrical patterns in both EF (left panel in A) and PF
912 (right panel in A). Intra-membrane particles (IMPs), which are transmembrane proteins,
913 were largely confined to the edges of polygonal areas. (B) Lipid droplets (LDs) adhered
914 tightly to the IMP-deficient raft-like domain, which bulged toward the vacuolar lumen.
915 The vacuolar membrane and microautophagic vesicles are indicated by double
916 arrowheads and arrows, respectively. Scale bar: 500 nm. (C) Labeling densities of
917 PtdIns(3)P in the vacuolar membrane of WT yeast and *cho1*Δ mutant. PtdIns(3)P
918 labeling was abundant in PF, and its density in the *cho1*Δ mutant was much lower
919 compared to that in WT yeast (see also Supplementary Fig. S10). Mean ± SE of three

920 independent experiments (>20 vacuoles were counted in each group in each
921 experiment). PtdIns(3)P labeling in EF and PF was compared to that in WT yeast. *t*-test:
922 n.s., not significant; ***$p < 0.001$.
923
924 **Figure 5. Microautophagic lipophagy in the starved *cho1*Δ mutant depends on the**
925 **expression of Vps27.**
926 (A) Micrographs depicting PtdIns(3)P labeling of macroautophagic bodies (blue and
927 green) and microautophagic vesicles (yellow and purple) within the vacuoles
928 of *cho1*Δ (a), *ubc4*Δ/*cho1*Δ (b), *ubc4*Δ (c), and *vps27*Δ/*cho1*Δ (d) mutants starved
929 supplemented with PMSF in the presence of Etn. Notably, no microautophagic vesicles
930 were detected in the vacuoles of starved *ubc4*Δ/*cho1*Δ (b) and *vps27*Δ/*cho1*Δ (d)
931 mutants, even with Etn supplementation. (C) According to the localization patterns of
932 PtdEtn (Fig. 3) and PtdIns(3)P (Fig. 2) labeling in EF and PF of the vesicular
933 membranes, the numbers of microautophagic vesicles in the vacuoles of the WT,
934 *psd1*Δ/*psd2*Δ, *cho1*Δ, *vps27*Δ/*cho1*Δ, *ubc4*Δ, and *ubc4*Δ/*cho1*Δ strains were determined.
935 Several microautophagic vesicles were detected in the vacuolar lumen of the starved
936 *cho1*Δ mutant in S(-NC) supplemented with PMSF in the presence (+Etn), but not in the
937 absence (-Etn) of Etn. Mean ± SE of three independent experiments (>30 vacuoles were
938 counted in each group in each experiment). The number of microautophagic vesicles in
939 the vacuole of each strain was compared to that in WT yeast. Dunnett's test: n.s., not
940 significant; *$p < 0.05$.
941
942 **Figure 6. Ubc4 is required for geometrical pattern of the vacuolar membrane.**
943 Micrographs of the PtdIns(3)P labeling in the vacuolar membrane of the *ubc4*Δ/*cho1*Δ

944 (A) and *vps27*Δ/*cho1*Δ (B) mutants starved supplemented with PMSF are shown. When
945 the *ubc4*Δ/*cho1*Δ and *vps27*Δ/*cho1*Δ mutants were starved in the presence of Etn, the
946 geometrical pattern was rarely observed in both the luminal (a) and cytoplasmic (b)
947 leaflets of the vacuolar membrane. Scale bar: 500 nm. (C) Proportion of geometrical
948 and no-domain patterns in the vacuolar membranes of WT yeast and the *cho1*Δ,
949 *psd1*Δ/*psd2*Δ, *ubc4*Δ/*cho1*Δ, and *vps27*Δ/*cho1*Δ mutants starved in the presence of Etn.
950 Ratios of the geometrical patterns in the starved *ubc4*Δ/*cho1*Δ and *vps27*Δ/*cho1*Δ
951 mutants were drastically decreased. Mean ± standard deviation (SD) of three
952 independent experiments (>100 vacuoles were counted in each group in each
953 experiment). Ratios of each pattern in WT, *psd1*Δ/*psd2*Δ, *ubc4*Δ/*cho1*Δ, and
954 *vps27*Δ/*cho1*Δ mutants were compared to that in the *cho1*Δ mutant. Dunnett's test: $*p <$
955 0.05.

956 **Supplemental information**

957 **Table S1. Yeast strains used in this study.**

958 Deletion mutants were generated using a standard PCR-based method.

959

960 **Figure S1. Outline of freeze-fracture EM.**

961 Replicas representing the outer (luminal) and inner (cytoplasmic) membrane leaflets are
962 called the EF and the PF, respectively. Fracture planes passing through the cytoplasm
963 and the extracellular space are shown by a dotted line.

964

965 **Figure S2. Macroautophagic body and microautophagic vesicle in the vacuole of**
966 **WT and *psd1*Δ/*psd2*Δ yeast strains.**

967 WT yeast (A) and the *psd1*Δ/*psd2*Δ (B) mutant were starved in S(-NC) medium
968 supplemented with PMSF for 5 h at 30 °C, both in the absence (a) and presence (b) of
969 ethanolamine (Etn). In WT yeast (A) and the *psd1*Δ/*psd2*Δ (B) mutant, two types of
970 vesicles were observed under both conditions: one with PtdIns(3)P labeling enriched in
971 the external face (EF, green) of vesicles in the vacuoles and another with labeling in the
972 peripheral face (PF, orange), but not the EF (purple). Double arrowheads, vacuole. Scale
973 bar, 500 nm.

974

975 **Figure S3. Forming processes of macroautophagic body and microautophagic**
976 **vesicle in the vacuole.**

977 Diagram showing how the macroautophagic body and microautophagic vesicle form in
978 the vacuole. LD, lipid droplet.

979

980 **Figure S4. Outline of the quick-freezing and freeze-fracture labelling (QF-FRL)**
981 **method of macroautophagic bodies in the vacuole.**
982 (1) Quick-freezing (QF): Live yeast cells are quickly frozen without ice crystal
983 formation. High-pressure and metal contact freezing methods were used in the present
984 study. In the high-pressure freezing method, samples are frozen using liquid nitrogen,
985 and the nucleation and growth of ice crystals were reduced by the brief application of a
986 pressure of 2100 bar. (2) Freeze-fracture: Frozen yeast cells are fractured at below −
987 130°C and under a high vacuum. Membranes are split into two leaflets, and the
988 hydrophobic interface (i.e. the acyl chain side of the phospholipid monolayer) is
989 exposed. (3) Vacuum evaporation: thin layers of carbon (C) and platinum (Pt) are
990 deposited onto the hydrophobic interface of membranes and physically stabilize the
991 molecules. Because platinum is evaporated at an oblique angle to the surface of the
992 specimen (45° in the present study), protruding structures block the evaporating atoms
993 to produce 'shadows' behind the structures. Areas deficient in the platinum deposition,
994 therefore, appear to be electron-lucent under EM. Transmembrane proteins are observed
995 as small bumps termed intra-membrane particles (IMPs). (4) SDS treatment. Specimens
996 are thawed and treated with a SDS solution to dissolve materials other than the lipid
997 monolayer and integral membrane proteins, which are in direct contact with the carbon
998 and platinum layer. This makes membrane proteins and lipid head groups accessible for
999 antibody labelling.
1000
1001 **Figure S5. Pathways of PtdEtn biosynthesis.**
1002 In *Saccharomyces cerevisiae*, PtdEtn is synthesized through three primary pathways: 1)
1003 the de novo or CDP-DAG pathway via mitochondrial Psd1, 2) the CDP-DAG pathway

1004 via Psd2, and 3) the CDP-ethanolamine branch of the Kennedy pathway.

1005

1006 **Fig. S6. Geometric patterns of the vacuolar membrane in starved *cho1*Δ mutants**

1007 **with ethanolamine supplementation.**

1008 The *cho1*Δ mutant was starved in S(-NC) medium for 5 h, either in the absence (A) or

1009 presence (B) of ethanolamine (Etn). In the absence of Etn, the vacuolar membrane

1010 displayed a typical round morphology in both the EF and PF fracture faces, as seen in

1011 (A). In contrast, in the presence of Etn, the vacuolar membrane exhibited distinct

1012 geometric patterns (B). PtdIns(3)P labeling was predominantly observed on the PF.

1013 Scale bar: 500 nm.

1014

1015 **Figure S7. GFP-Atg8 processing assay under nitrogen-deficient SD(-N) conditions.**

1016 Degradation of GFP-Atg8 via macroautophagy in the *cho1*Δ mutant. Wild-type (WT)

1017 yeast and the *cho1*Δ mutant, transformed with a plasmid expressing GFP-Atg8 under

1018 the control of the *CUP1* promoter, were cultured in SMD-Ura medium at 30°C to mid-

1019 log phase. The cultures were then divided into three aliquots: one was incubated in YPD

1020 medium for 4 hours at 30°C, while the other two were shifted to SD(-N) medium

1021 without PMSF and cultured for 4 h at 30°C, either in the presence or absence of 3 mM

1022 ethanolamine (Etn). Samples were collected before (+N) and after (-N) nitrogen

1023 starvation. Bands corresponding to full-length GFP-Atg8 and free GFP are shown.

1024 Impaired GFP-Atg8 degradation was observed in the *cho1*Δ mutant regardless of Etn

1025 supplementation.

1026

1027 **Fig. S8. The vacuolar lumen contained vesicles associated with clusters of IMPs.**

1028 The cho1Δ mutant was starved for 5 hr in S(-NC) supplemented with PMSF. A raft-like
1029 domain gave rise to a balloon-shaped projection extending into the vacuolar lumen.
1030 Clusters of IMPs appeared as a ring at the neck of this structure (indicated by arrows).
1031 The labelings of PtdIns(3)P were observed in the PF, but not EF, of the microautophagic
1032 vesicles.
1033
1034 **Figure S9. PtdIns(4)P labeling in vesicle membranes within the vacuole of starved**
1035 **WT and *cho1*Δ yeast.**
1036 (A) Electron micrographs showing PtdIns(4)P labeling on the PF and EF of
1037 macroautophagic body membranes (blue and green) and microautophagic vesicle
1038 membranes (orange and purple) within the vacuole of WT and *cho1Δ* mutant yeast
1039 starved in S(-NC) supplemented with PMSF in the presence of ethanolamine (Etn).
1040 Scale bar: 500 nm. (B) Quantification of PtdIns(4)P labeling density on the PF of
1041 microautophagic vesicles and the EF of macroautophagic bodies in the vacuoles of
1042 starved WT and *cho1Δ* yeast. Labeling density on the PF of microautophagic vesicles
1043 and the EF of macroautophagic bodies was significantly higher than on the opposite
1044 membrane faces (EF and PF, respectively), indicating that the vesicles in the vacuole of
1045 starved *cho1Δ* cells are predominantly microautophagic in origin. Data represent mean
1046 ± SE from three independent experiments (>30 vesicles analyzed per group in each
1047 experiment). Statistical analysis was performed using a *t*-test: ***$p < 0.001$.
1048
1049 **Figure S10. Decrease in the PtdIns(3)P labelings in the vacuolar membrane of**
1050 ***cho1*Δ mutant.**
1051 Micrograph shows the PtdIns(3)P labelings on the PF in the vacuolar membranes of WT

1052 (A) and *cho1*Δ (B) strains starved in S(-NC) supplemented with PMSF in the presence
1053 of ethanolamine (Etn). The PtdIns(3)P labeling in the vacuolar membrane of *cho1*Δ
1054 mutant was much lower than that of WT yeast.
1055
1056 **Figure S11. Outline of the QF-FRL method of microautophagic vesicles in the**
1057 **vacuole.**
1058 The detail of the QF-FRL method is described in the figure legend of Fig. S4.
1059
1060 **Figure S12. IMP-deficient raft-like domains in the vacuolar membrane of *ubc4*Δ**
1061 **mutant after starvation.**
1062 The IMP-deficient raft-like domains were observed both in the PF (left) and the EF (right)
1063 of the vacuolar membrane in the starved *ubc4*Δ mutant supplemented with PMSF. The PF
1064 is densely labeled for PtdIns(3)P both in the IMP-rich and IMP-deficient domains. Scale
1065 bar: 500 nm.
1066
1067 **Figure S13. Distribution of PtdEtn in the vacuolar membrane of the starved WT**
1068 **and *cho1*Δ strain.**
1069 (A) PtdEtn was localized in both the EF and PF leaflets in the vacuolar membrane of the
1070 starved WT yeast supplemented with PMSF in the presence of Etn in the medium, and
1071 the PtdEtn labeling density was much higher in the PF than that in the EF of WT (B). In
1072 contrast to the WT yeast, the PtdEtn labeling was detected on the PF, but not the EF, in
1073 the vacuolar membrane of the starved *cho1*Δ in the presence of Etn. Scale bar: 500 nm.
1074 Mean ± SE of three independent experiments (>30 vacuoles were counted in each
1075 experiment). The PtdEtn labeling of the *cho1*Δ mutant was compared to that of the WT

1076 yeast. *t-test*: n.s., not significant; *** $p < 0.001$.

1077

1078 **Fig. S14. Intraluminal vesicles (ILVs) within the multivesicular bodies (MVBs) of**

1079 **starved *ypt7*Δ mutants and in the vacuolar lumen of starved *pep4*Δ mutants.**

1080 The *ypt7*Δ and *pep4*Δ mutants were subjected to starvation in S(-NC) medium without

1081 PMSF at 30°C for 5 hours. (A) In starved *ypt7*Δ mutants, intraluminal vesicles (ILVs),

1082 appearing as small, irregularly contoured structures (indicated by arrows in the right

1083 panel), were observed within the multivesicular bodies (MVBs) of endosomes using the

1084 freeze-fracture EM method. (B) In starved *pep4*Δ cells, ILVs along with accumulated

1085 macroautophagic bodies labeled for PtdSer on both the EF and PF were detected within

1086 the vacuole. The morphology of these rugged structures was indistinguishable from that

1087 of ILVs observed in the endosomal MVBs of *ypt7*Δ mutants (see also Figure 6—figure

1088 supplement 1 in [10]).

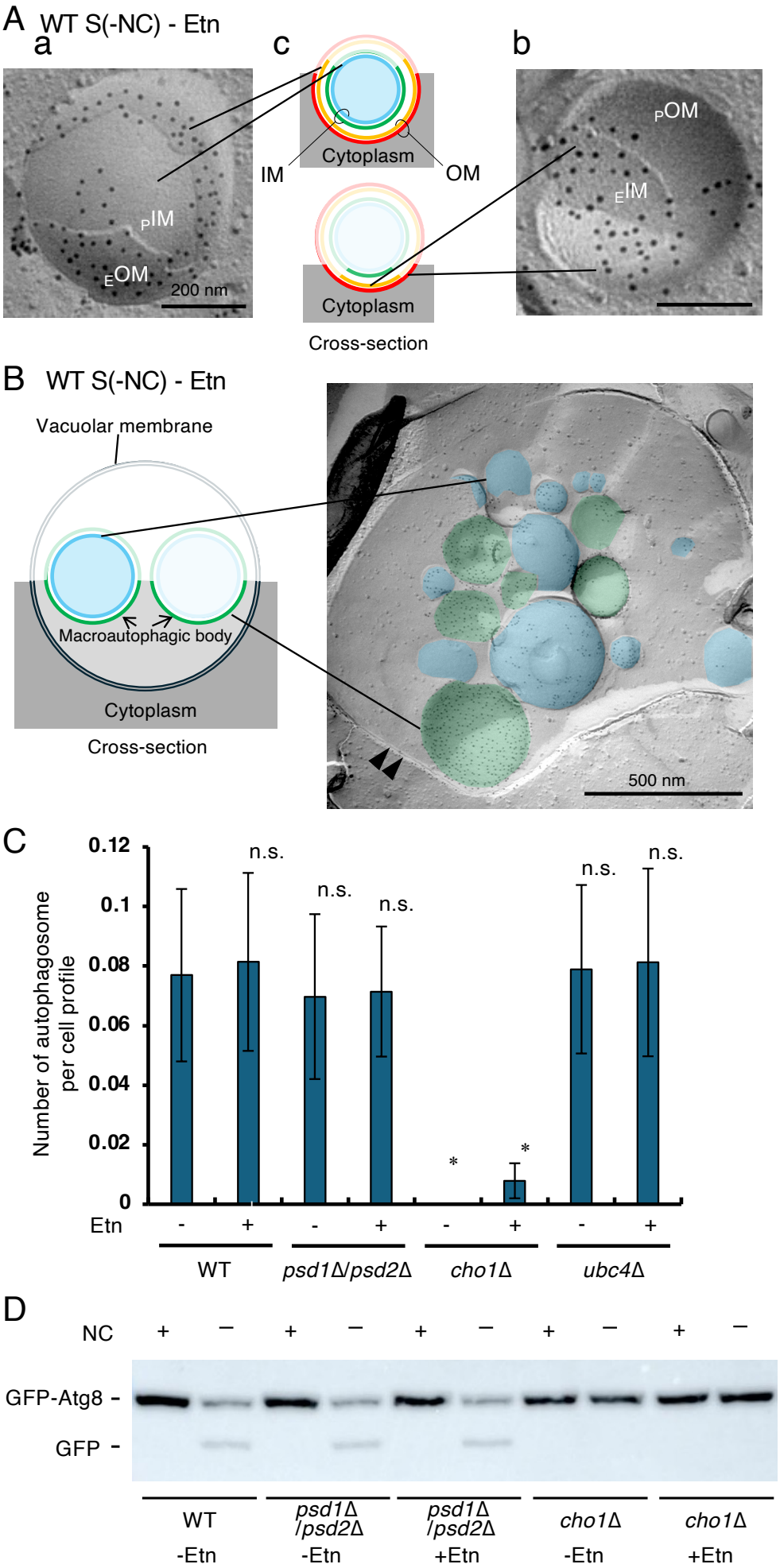
A WT S(-NC) - Etn
a
c
b
PIM
EOM
200 nm
IM
OM
Cytoplasm
Cytoplasm
Cross-section
POM
EIM
B WT S(-NC) - Etn
Vacuolar membrane
Macroautophagic body
Cytoplasm
Cross-section
500 nm
C
Number of autophagosome per cell profile
0.12
0.1
0.08
0.06
0.04
0.02
0
n.s.
n.s.
n.s.
n.s.
n.s.
*
*
Etn
-
+
-
+
-
+
-
+
WT
psd1Δ/psd2Δ
cho1Δ
ubc4Δ
D
NC
+
−
+
−
+
−
+
−
+
−
GFP-Atg8
GFP
WT -Etn
psd1Δ /psd2Δ -Etn
psd1Δ /psd2Δ +Etn
cho1Δ -Etn
cho1Δ +Etn

Fig. 1

A WT

a S(-NC) – Etn

b S(-NC) + Etn

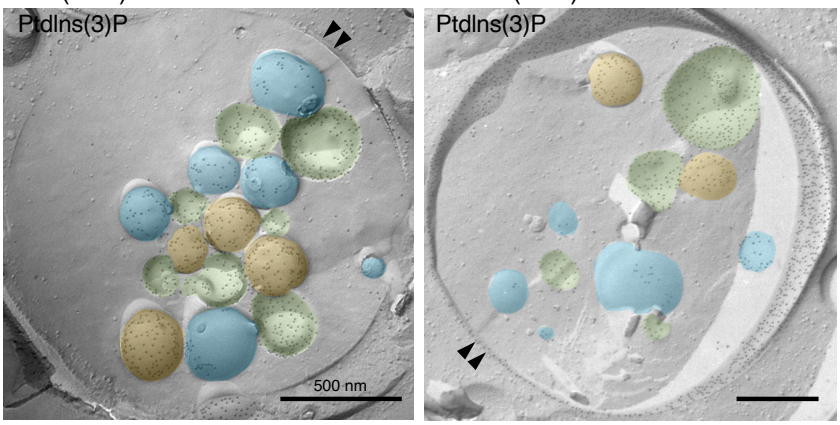

B *psd1*Δ / *psd2*Δ

a S(-NC) – Etn

b S(-NC) + Etn

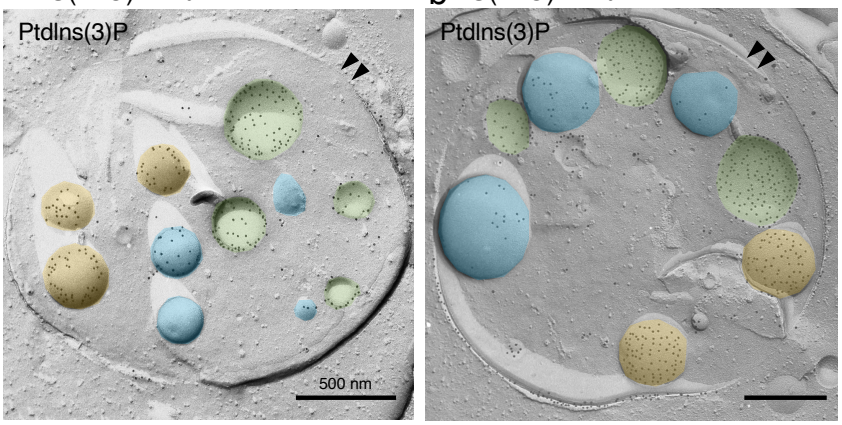

C *cho1*Δ

a S(-NC) – Etn

b S(-NC) + Etn

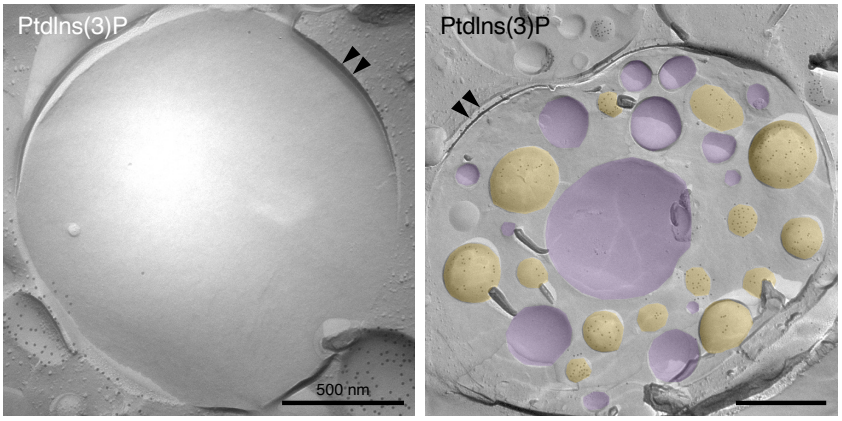

D Vesicle membrane in vacuole

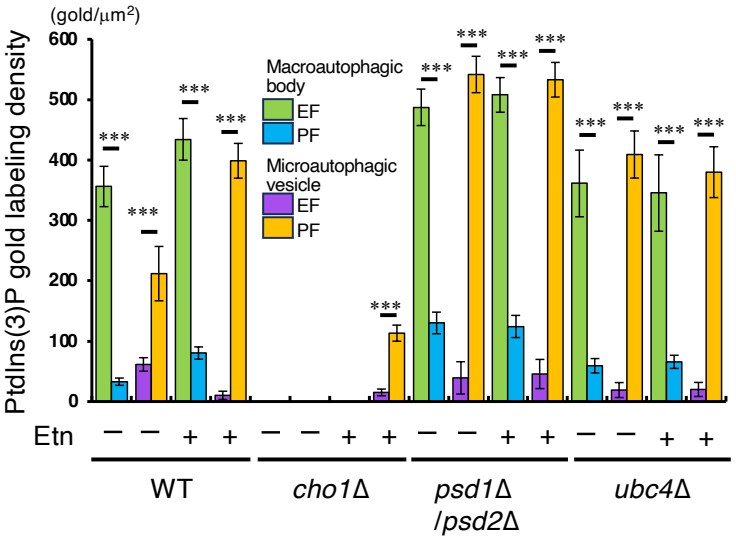

Fig. 2

A WT S(-NC) + Etn

a

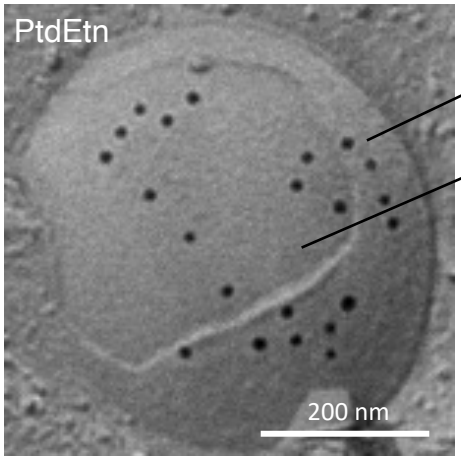

b

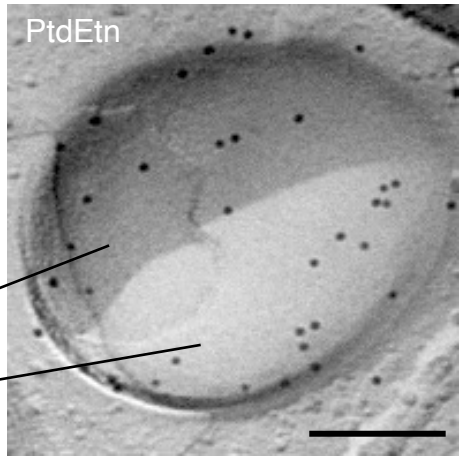

$_{E}$OM

$_{P}$IM

$_{E}$IM

$_{P}$OM

B

a WT S(-NC) + Etn

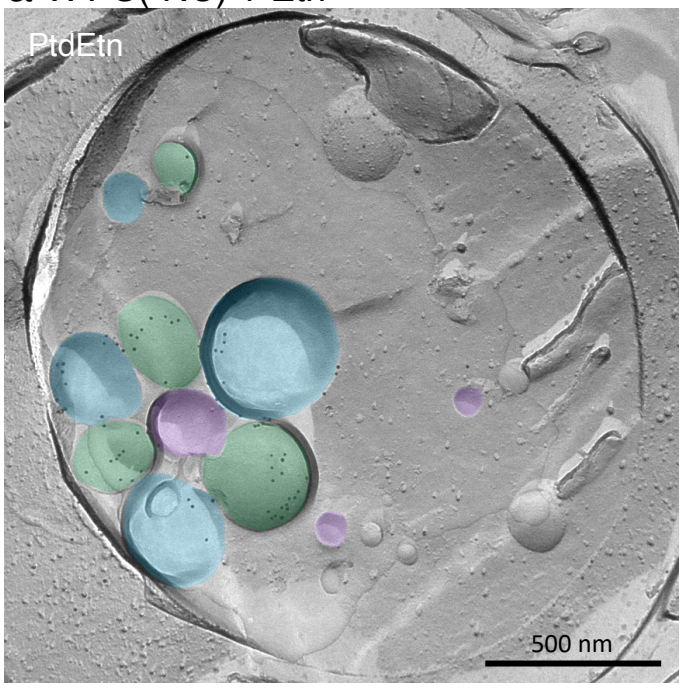

b *cho1*Δ S(-NC) + Etn

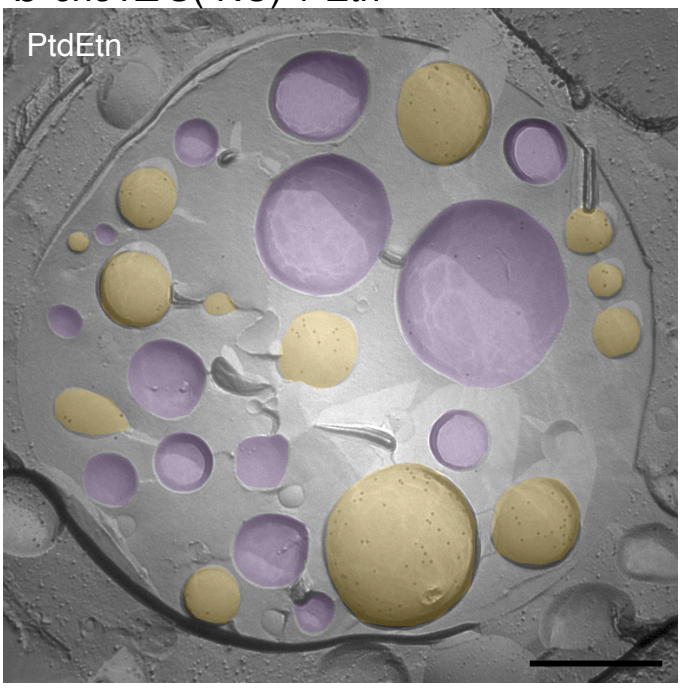

C

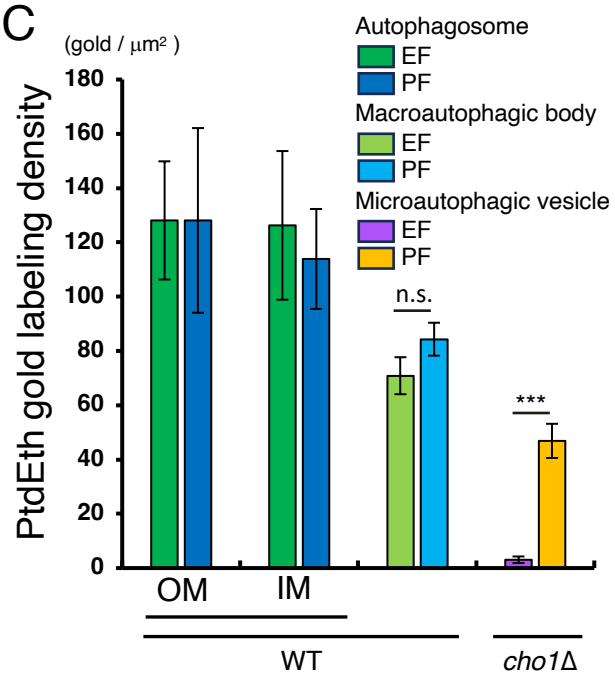

D Macroautophagic body in vacuole

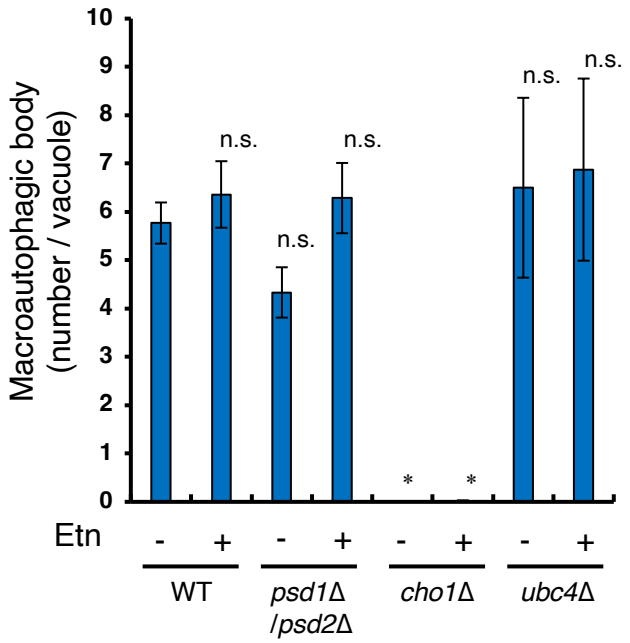

Fig. 3

A Vacuolar membrane in starved *cho1*Δ (+Etn)

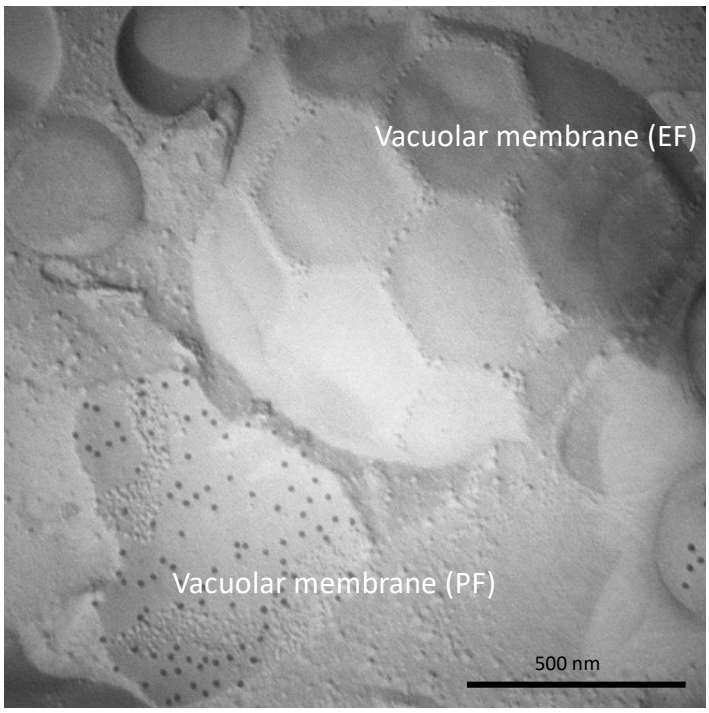

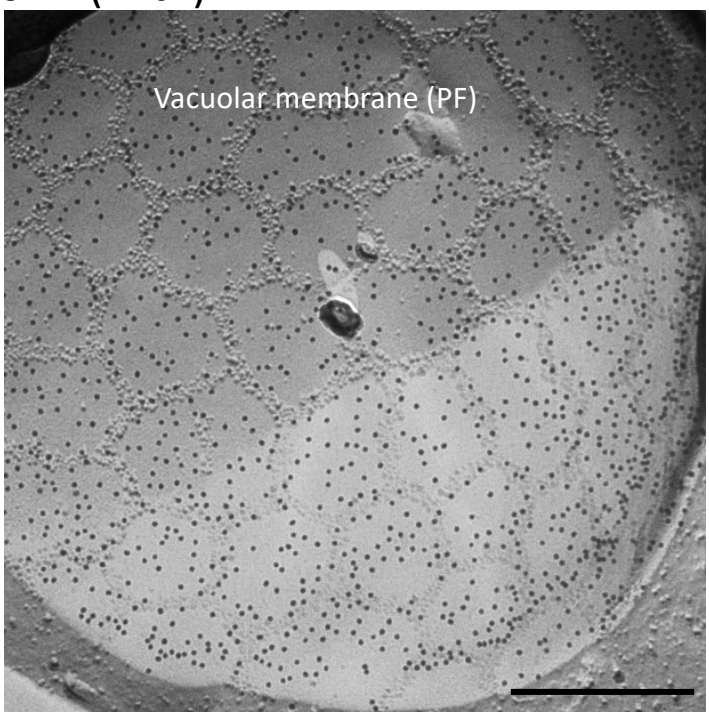

B Microautophagic vesicle

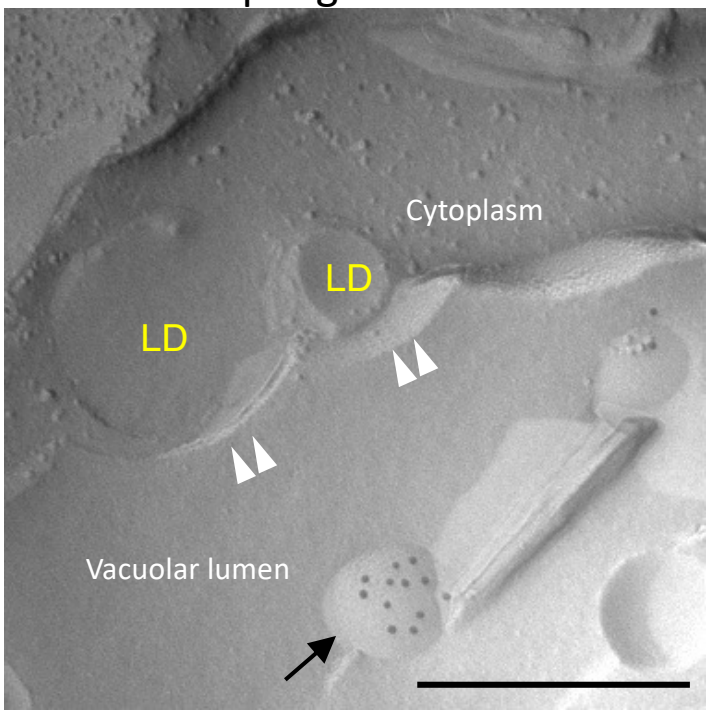

C PtdIns(3)P in vacuolar membrane

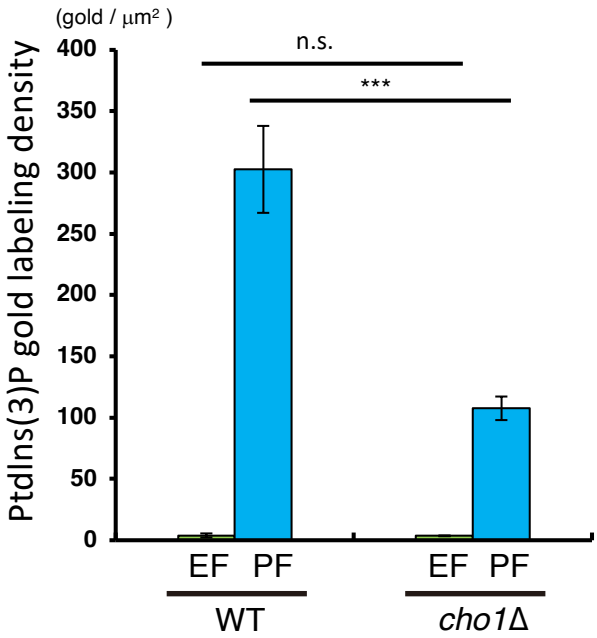

Fig. 4

A a *cho1Δ* S(-NC) + Etn

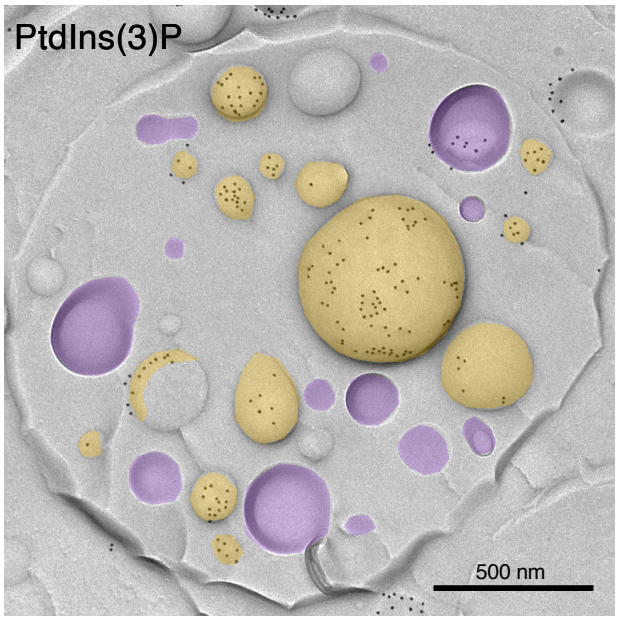

b *ubc4Δ/cho1Δ* S(-NC) + Etn

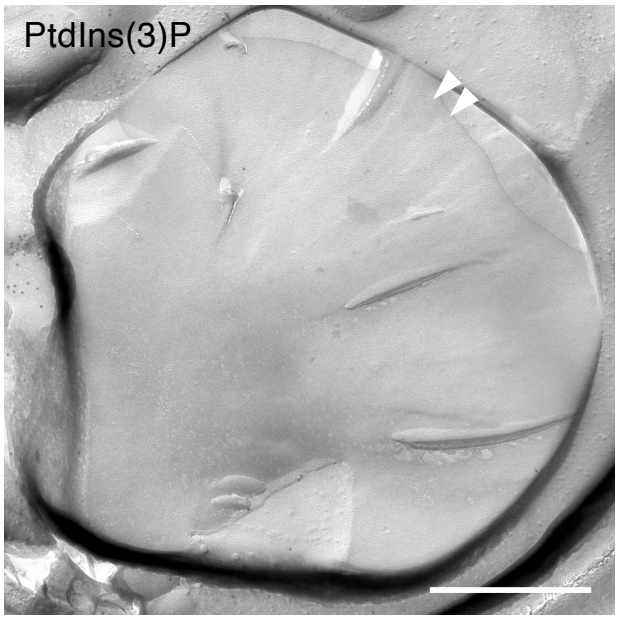

c *ubc4Δ* S(-NC) + Etn

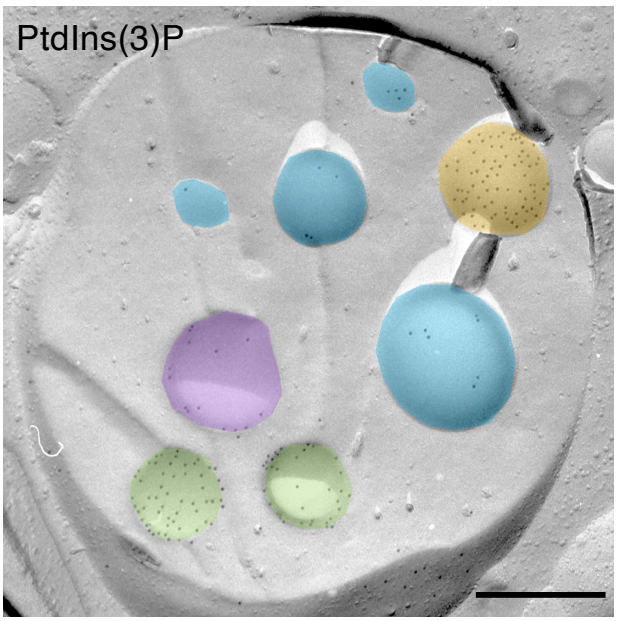

d *vps27Δ/cho1Δ* S(-NC) + Etn

B

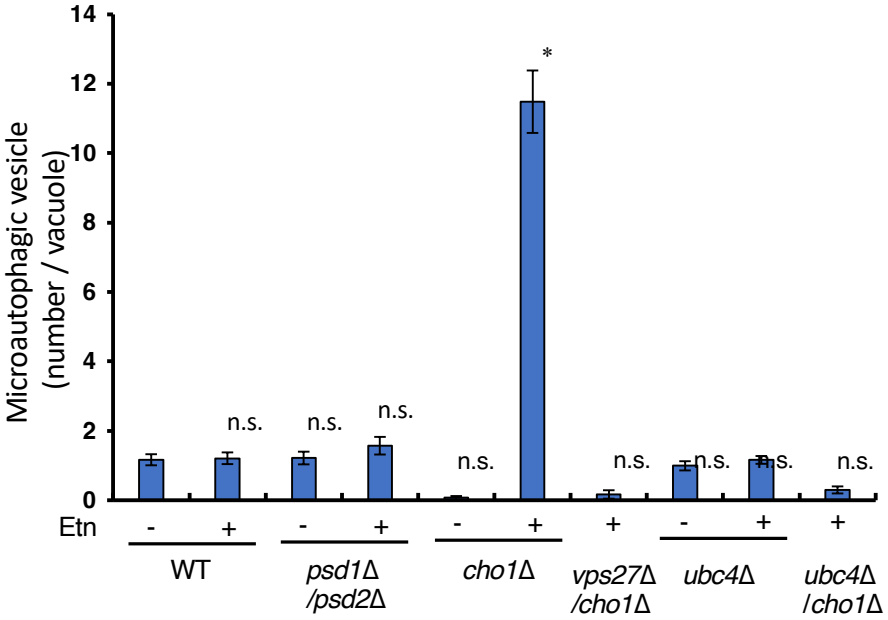

Fig. 5

A *ubc4Δ/cho1Δ* S(-NC) +Etn

a Luminal leaflet (EF) of vacuole

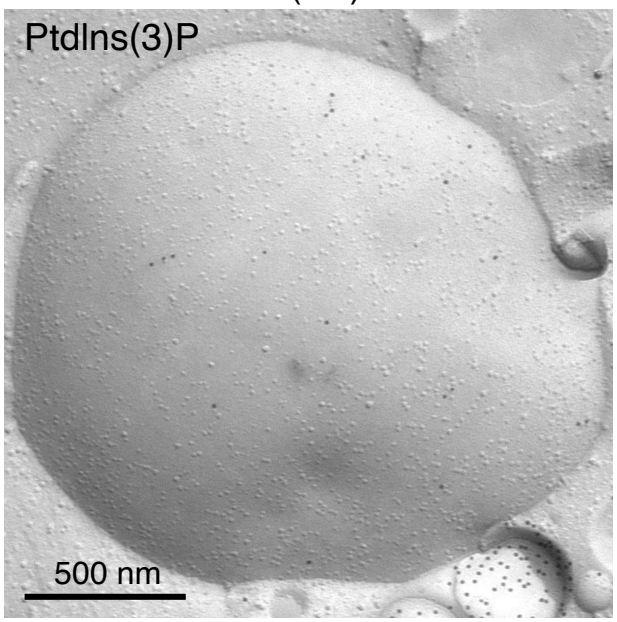

B *vps27Δ/cho1Δ* S(-NC) +Etn

Luminal leaflet (EF) of vacuole

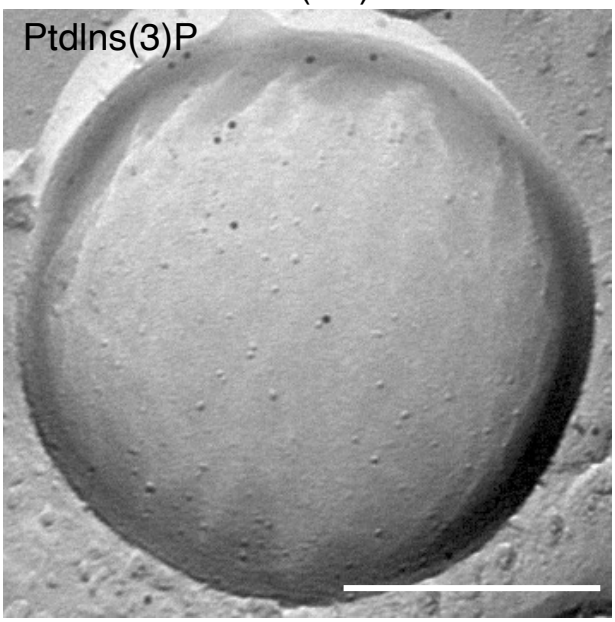

b Cytoplasmic leaflet (PF) of vacuole

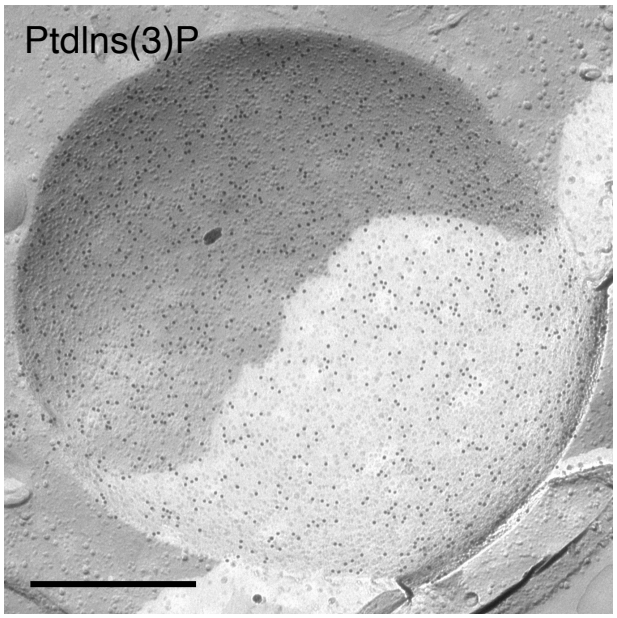

C

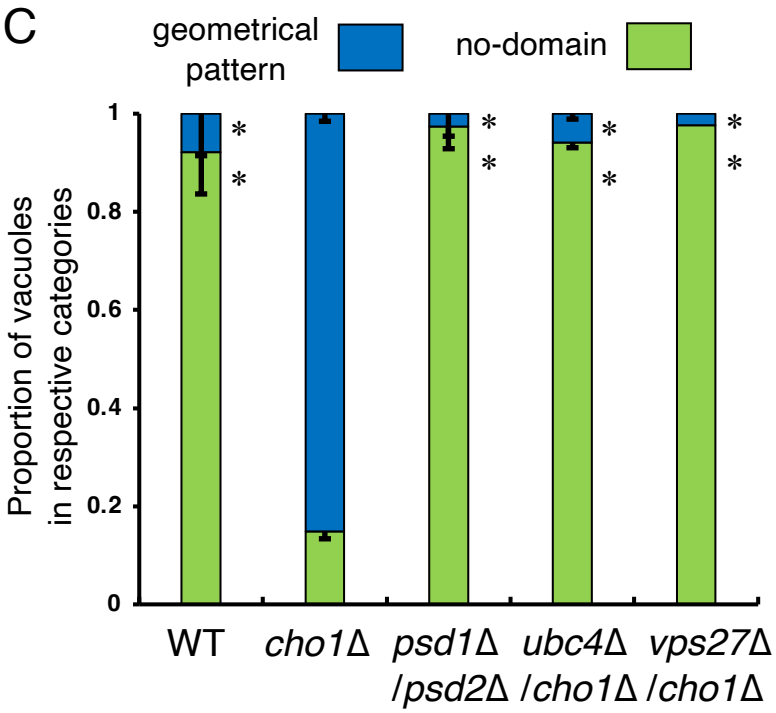

Fig. 6

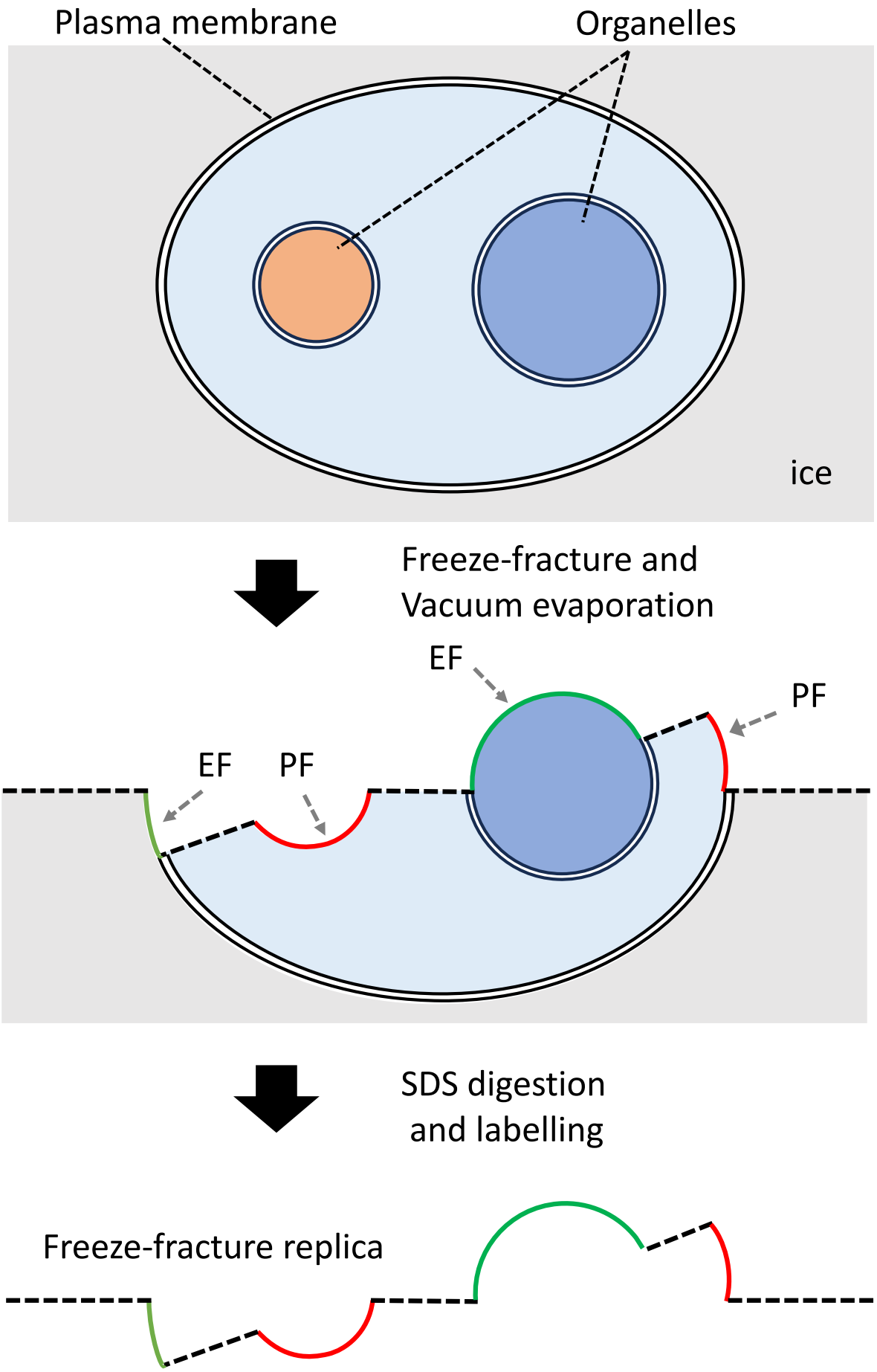
Plasma membrane
Organelles
ice
Freeze-fracture and
Vacuum evaporation
EF
PF
EF
PF
SDS digestion
and labelling
Freeze-fracture replica

Fig. S1

A WT

a S(-NC) – Etn

b S(-NC) + Etn

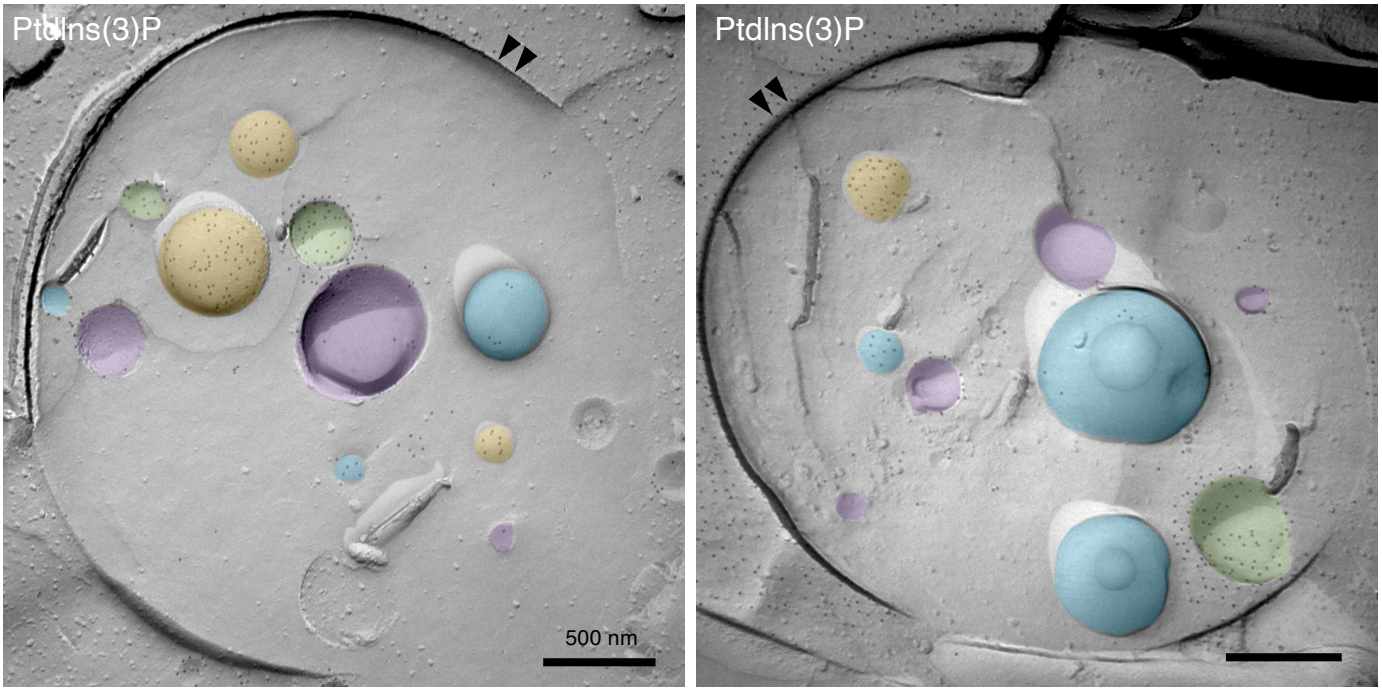

B *psd1*Δ / *psd2*Δ

a S(-NC) – Etn

b S(-NC) + Etn

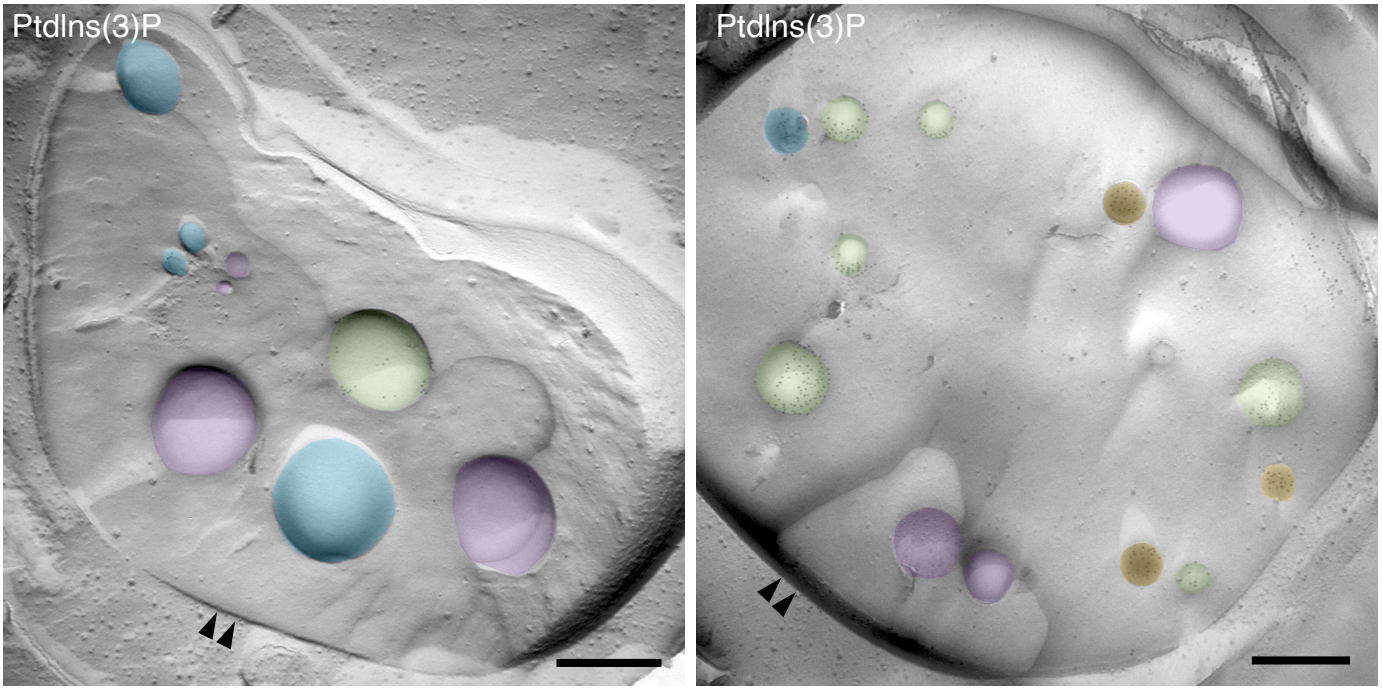

Fig. S2

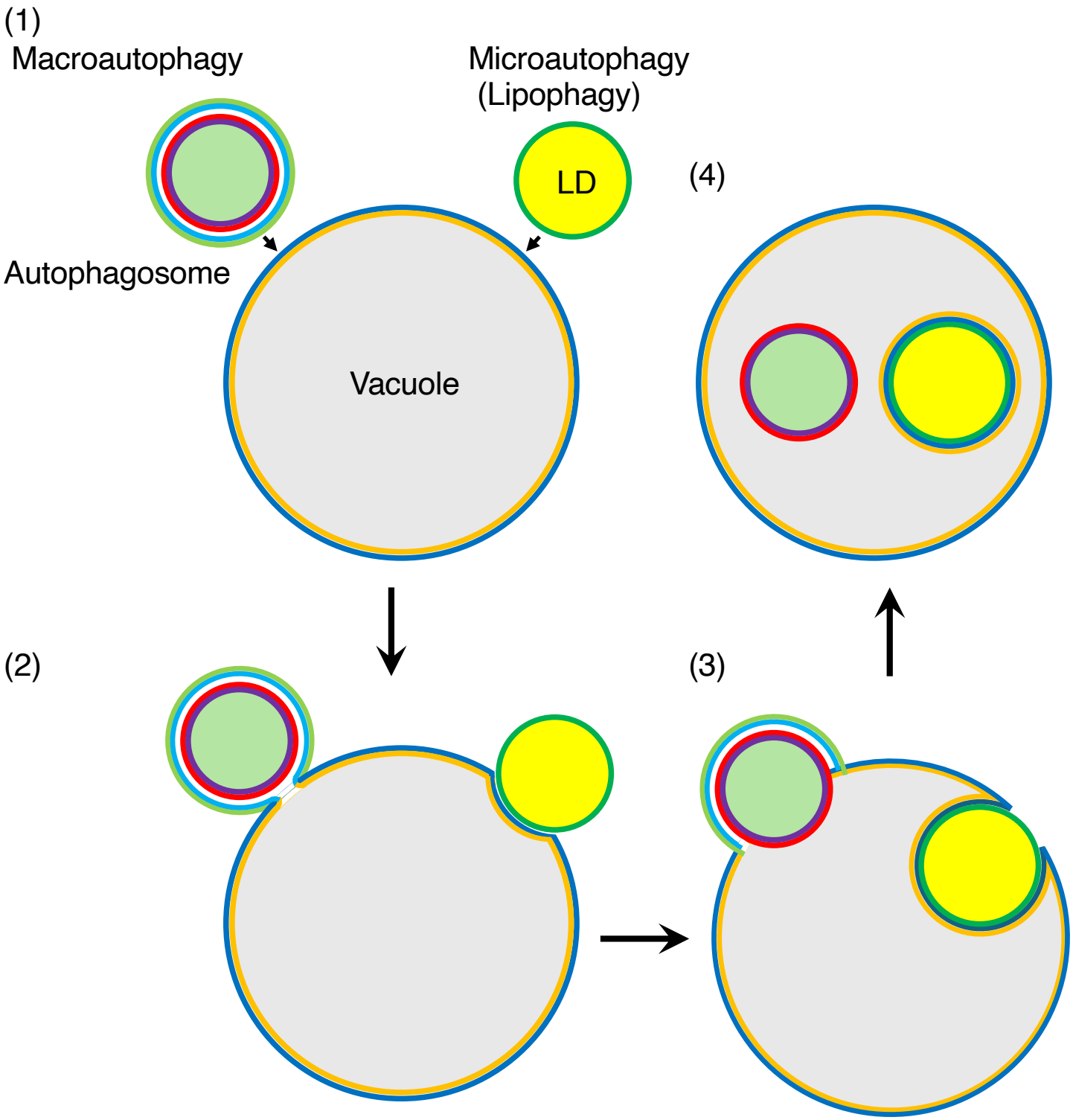
(1)
Macroautophagy
Microautophagy
(Lipophagy)
LD
(4)
Autophagosome
Vacuole
(2)
(3)

Fig. S3

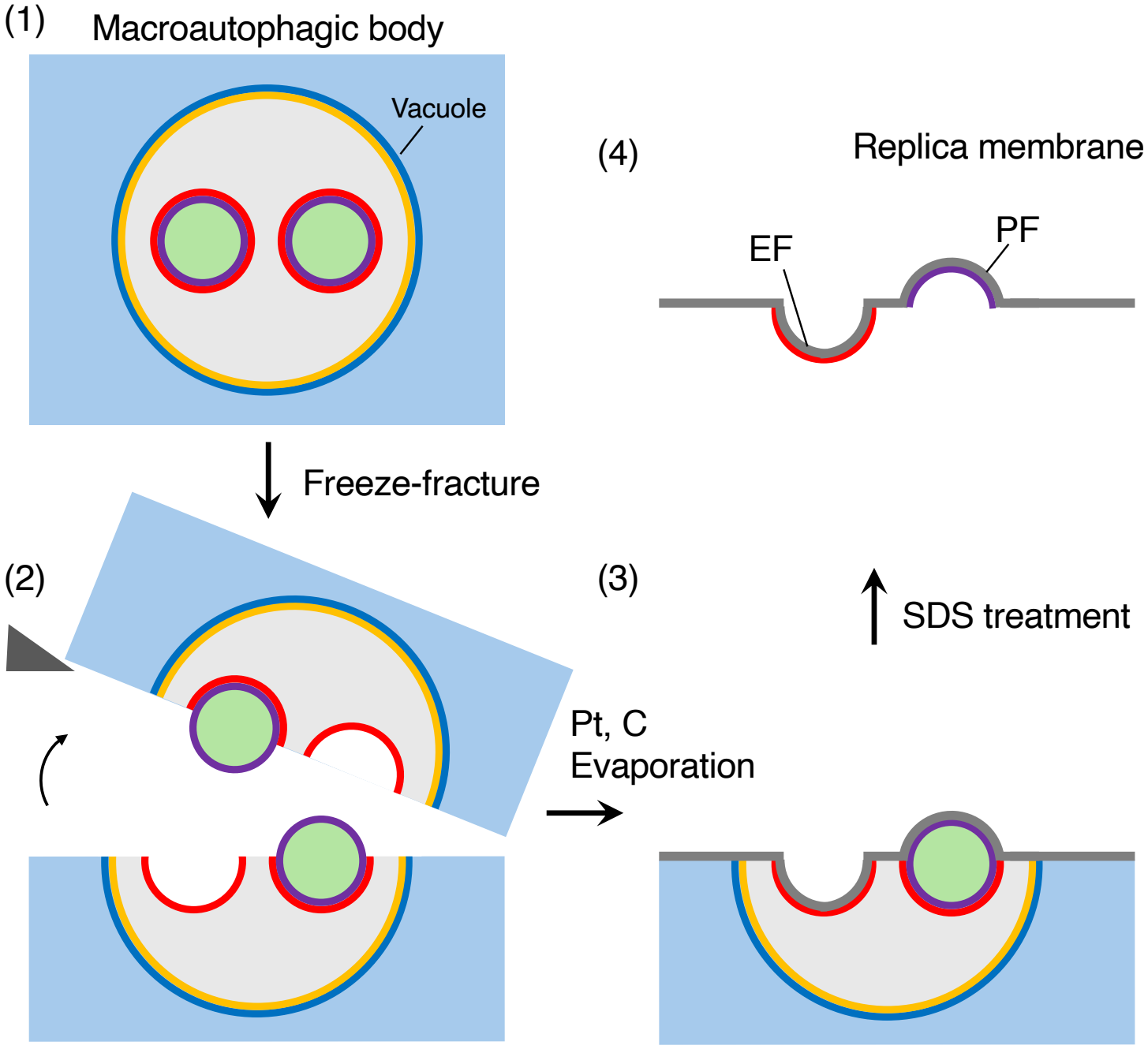
(1)
Macroautophagic body
Vacuole
Freeze-fracture
(2)
(3)
SDS treatment
Pt, C
Evaporation
(4)
Replica membrane
EF
PF

Fig. S4

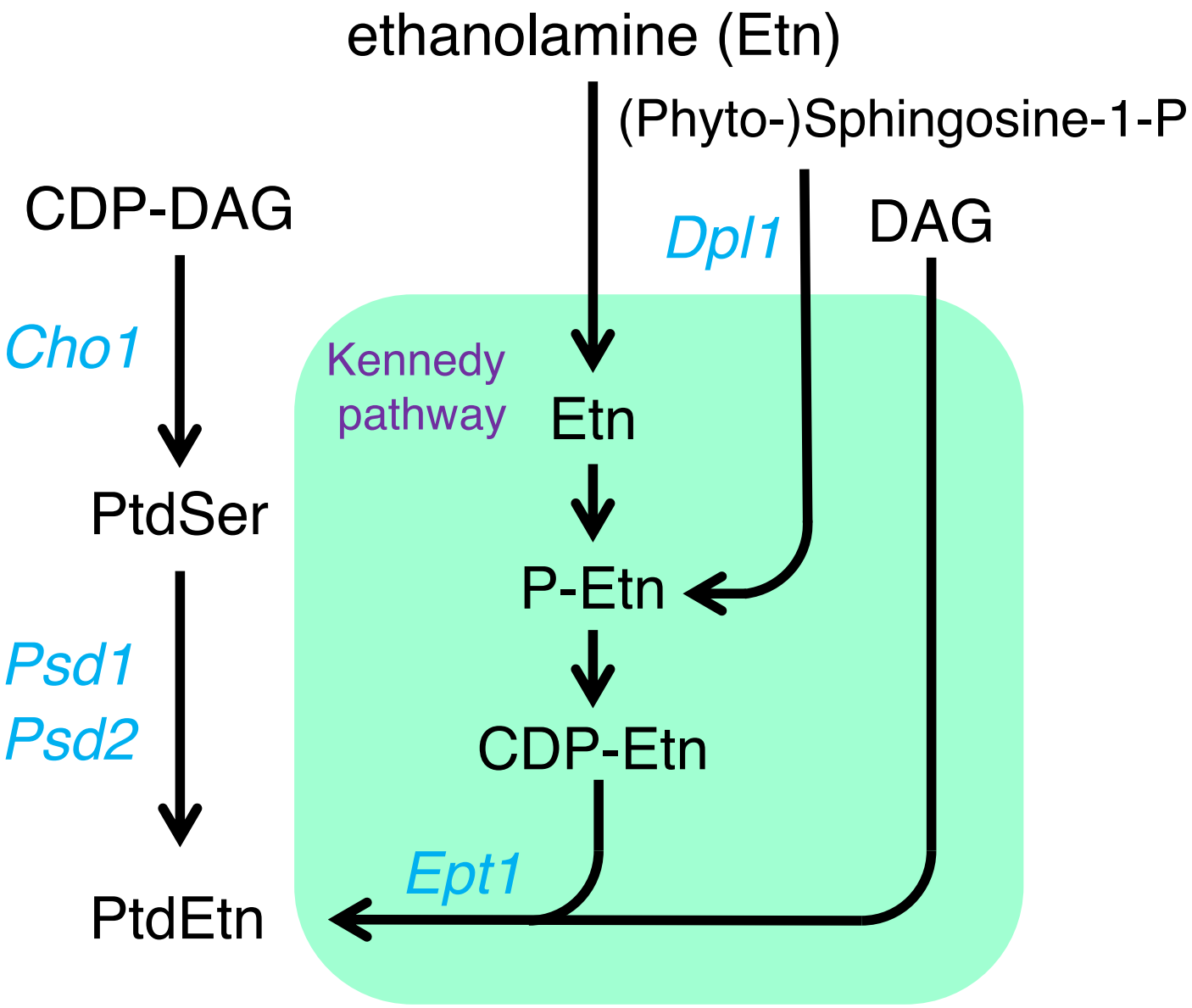
ethanolamine (Etn)
(Phyto-)Sphingosine-1-P
CDP-DAG
Dpl1
DAG
Cho1
Kennedy
pathway
Etn
PtdSer
P-Etn
Psd1
Psd2
CDP-Etn
Ept1
PtdEtn

Fig. S5

A Vacuolar membrane in starved *cho1*Δ (- Etn)

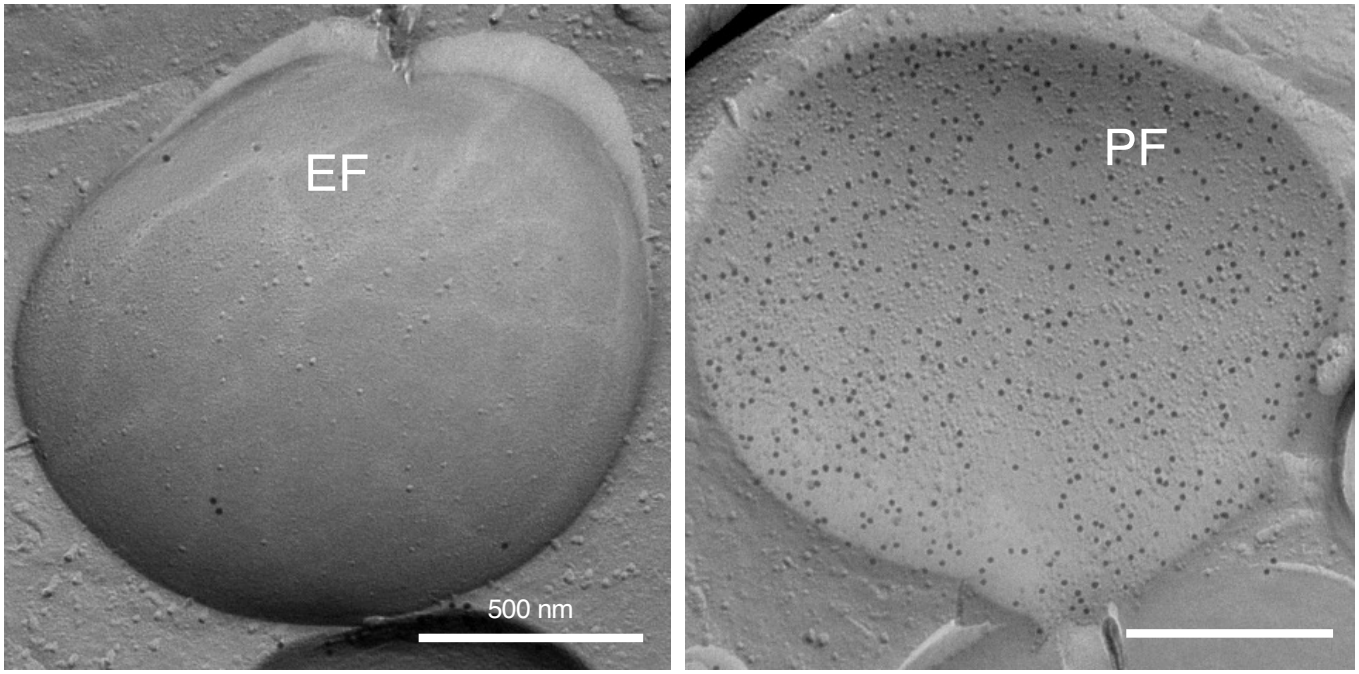

B Vacuolar membrane in starved *cho1*Δ (+ Etn)

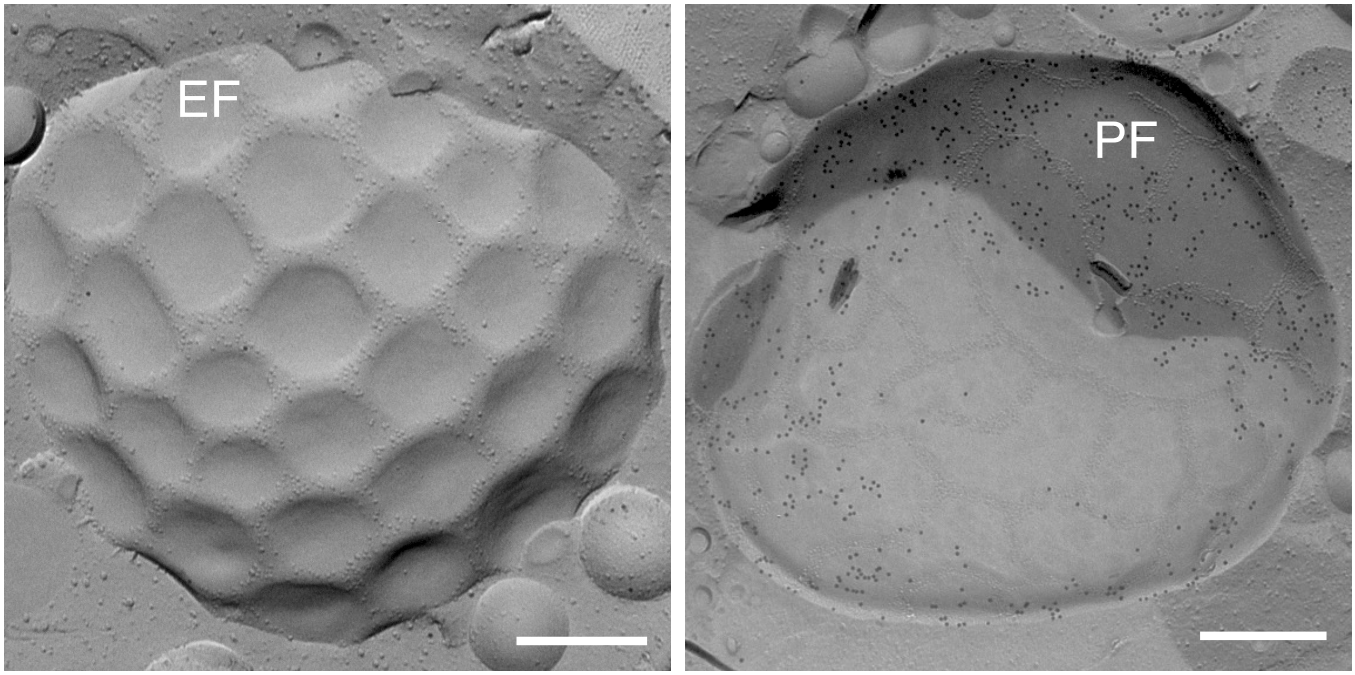

Fig. S6

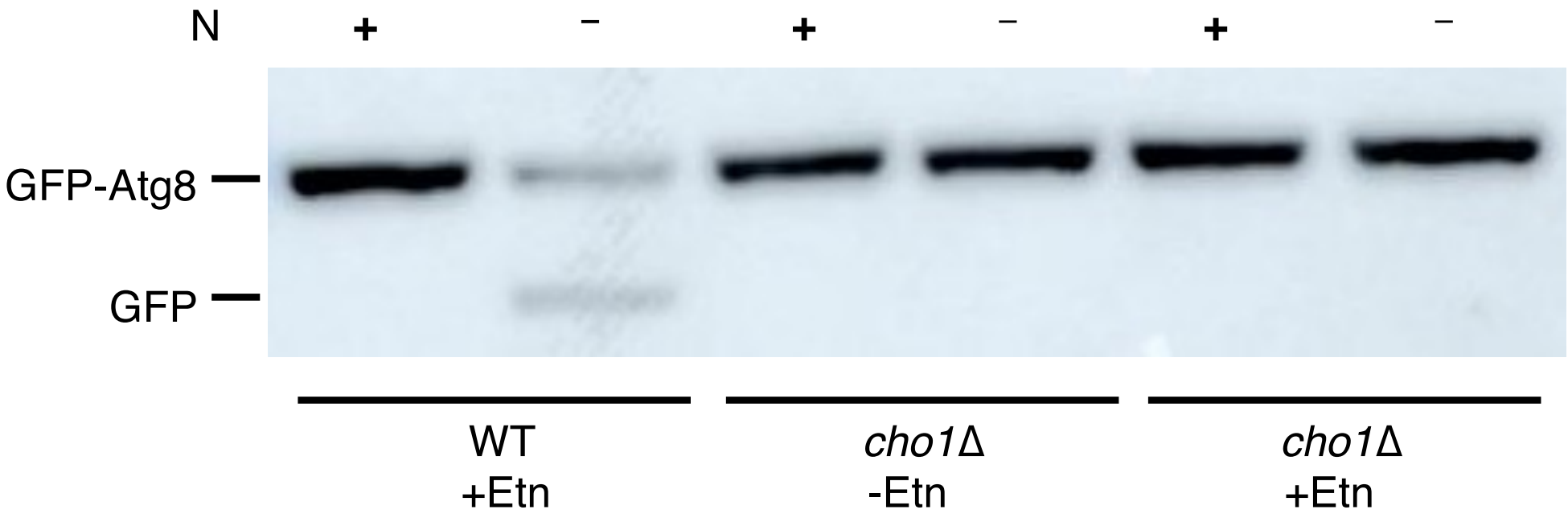

Fig. S7

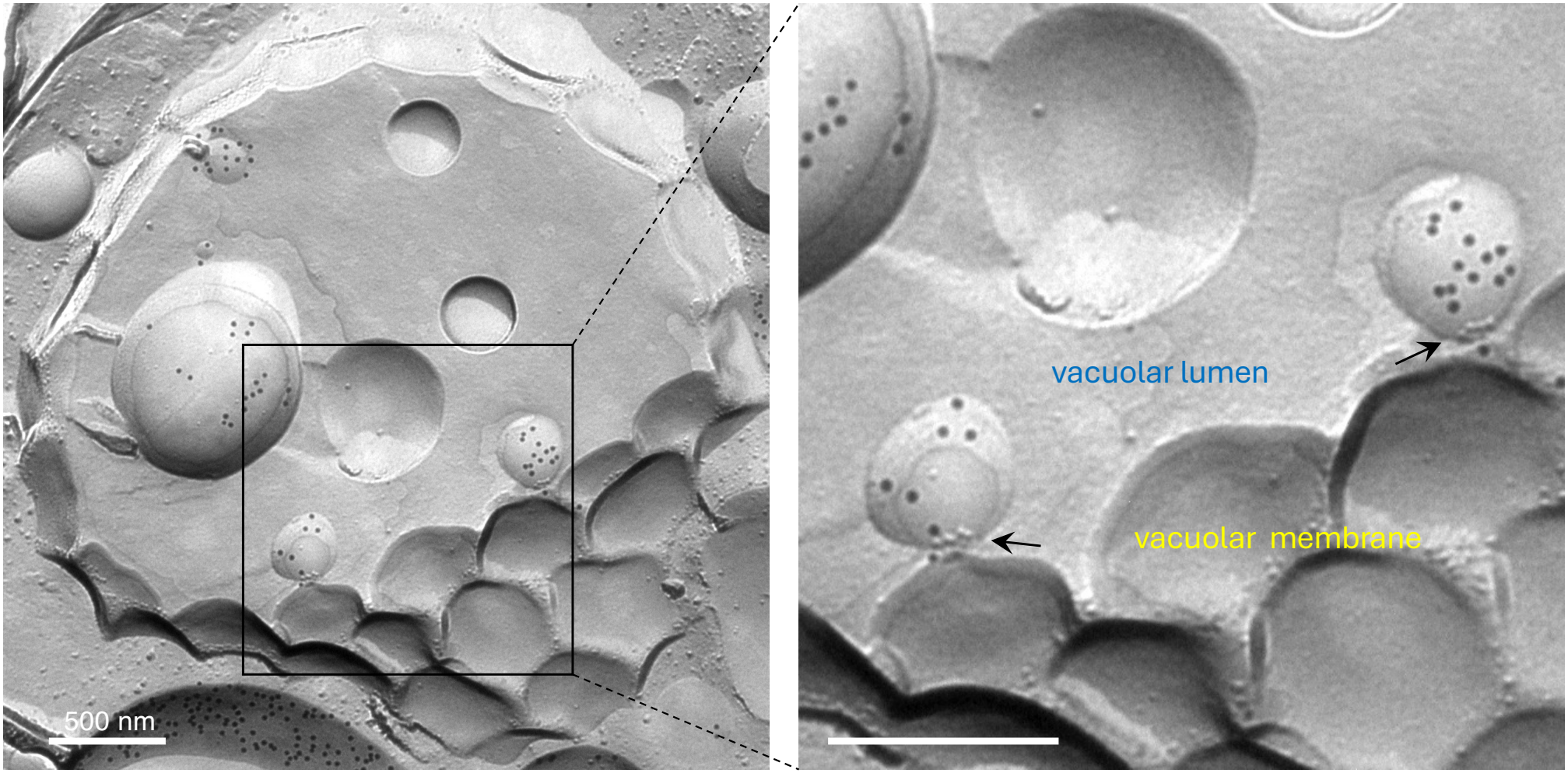

Fig. S8

A PtdIns(4)P in macroautophagic body and microautophagic vesicle

a WT

b *cho1*Δ

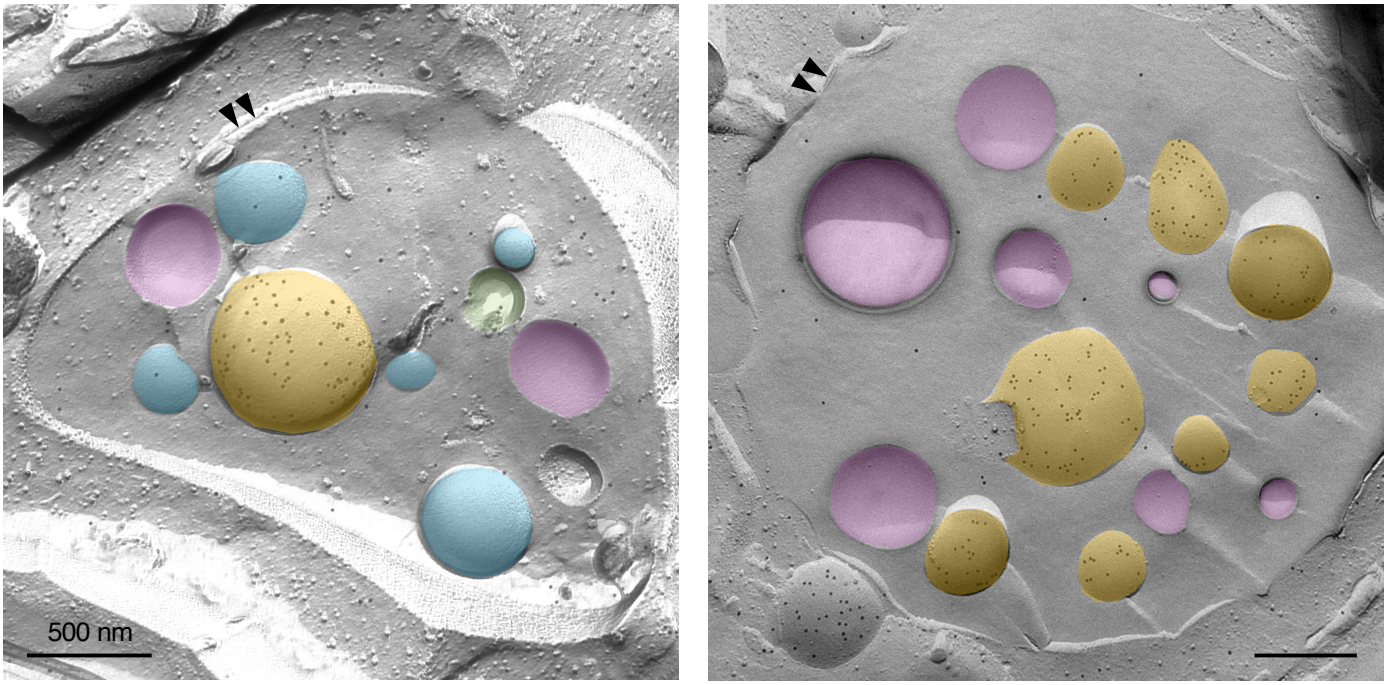

B Vesicular membranes in vacuole

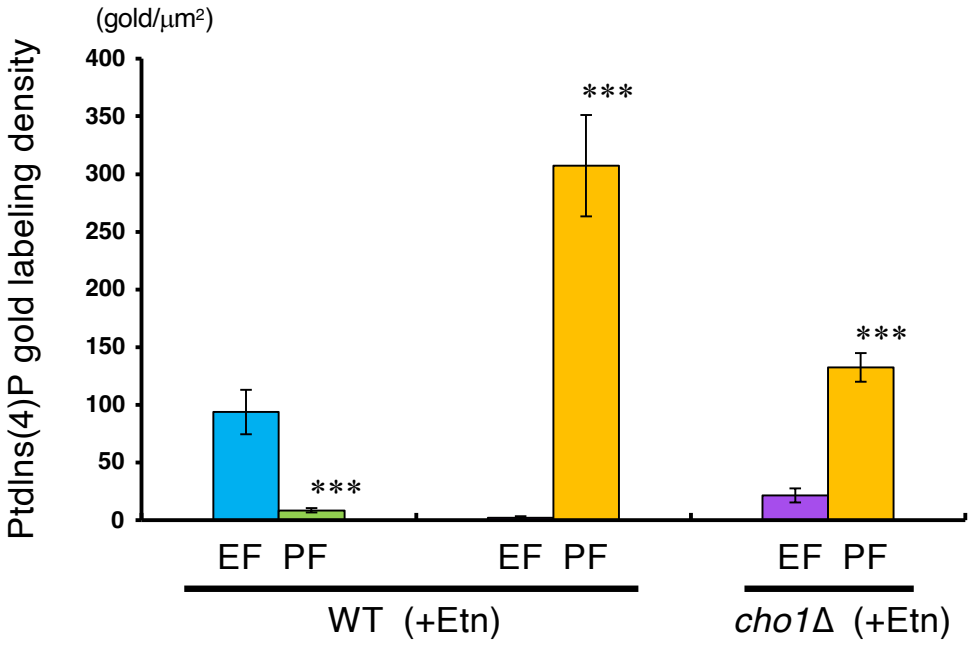

Fig. S9

A WT

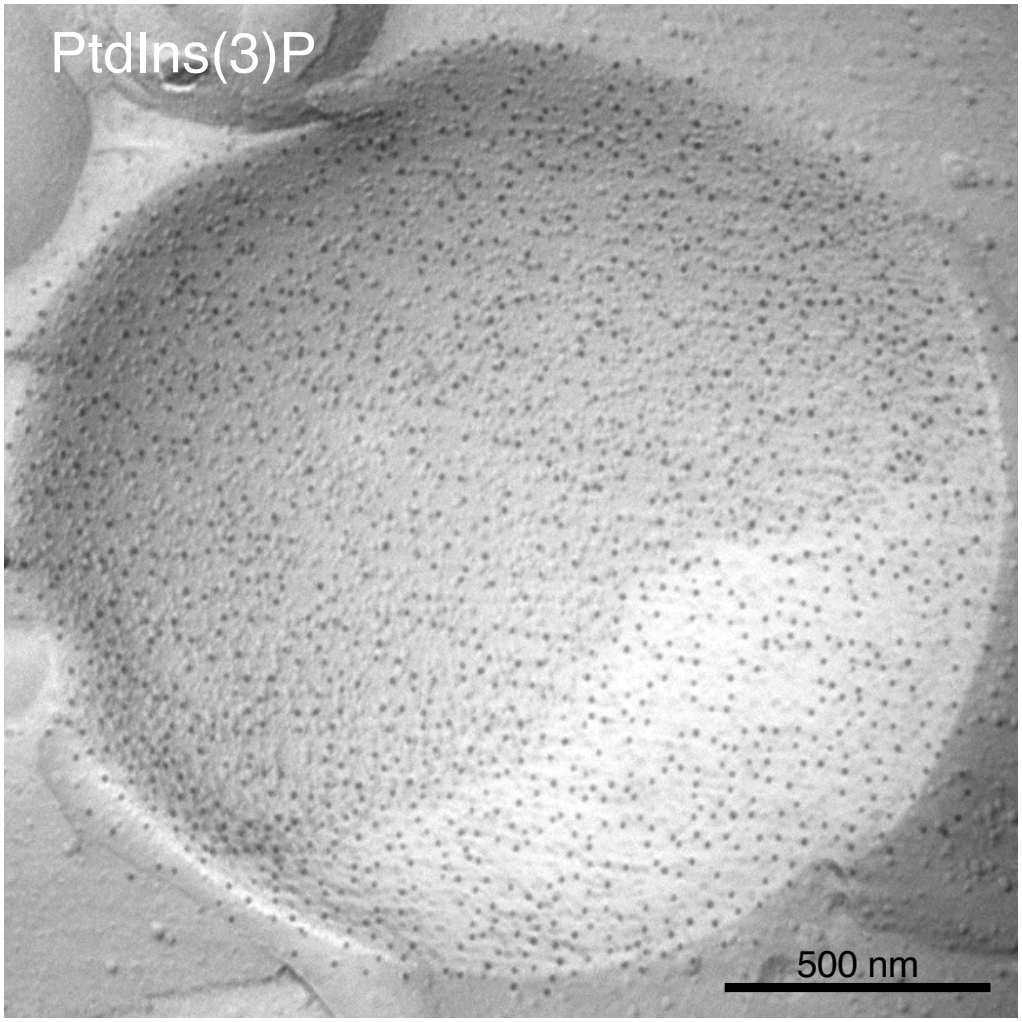

B *cho1Δ*

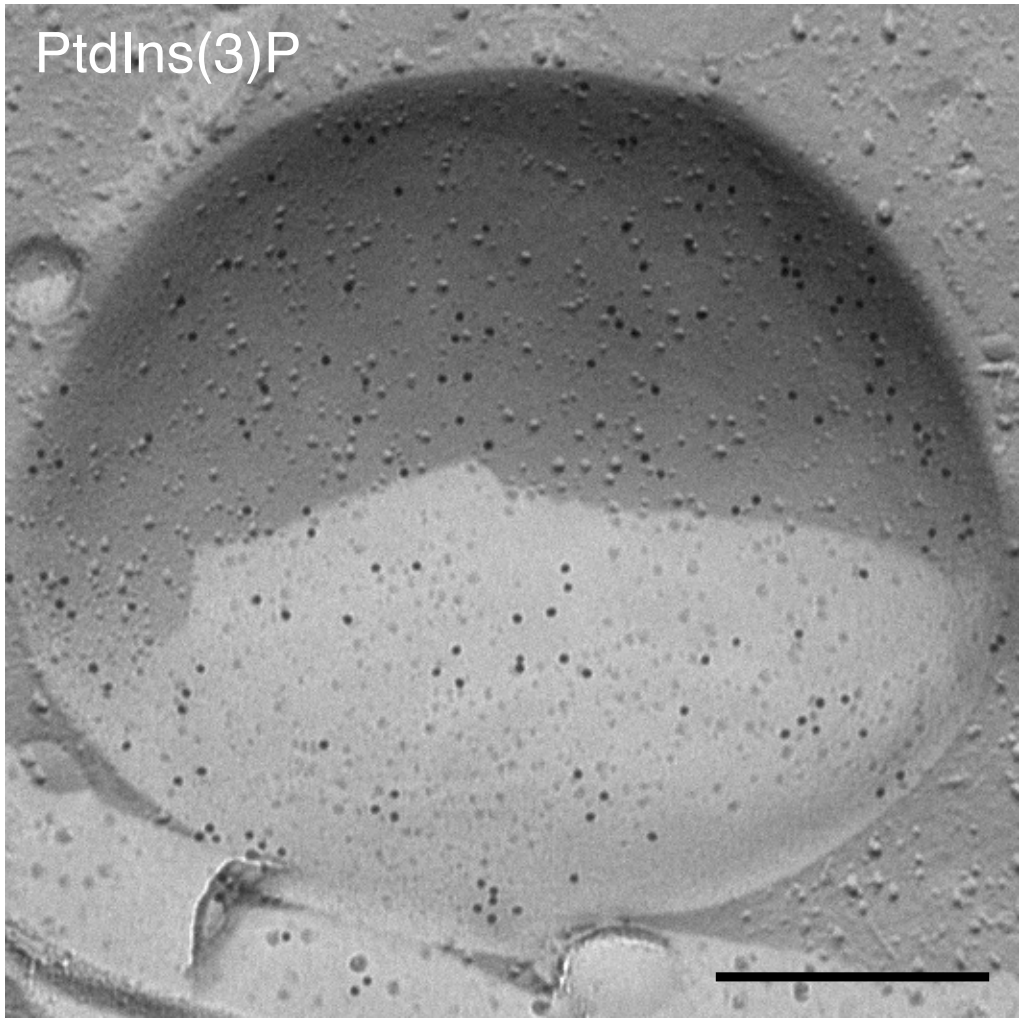

Fig. S10

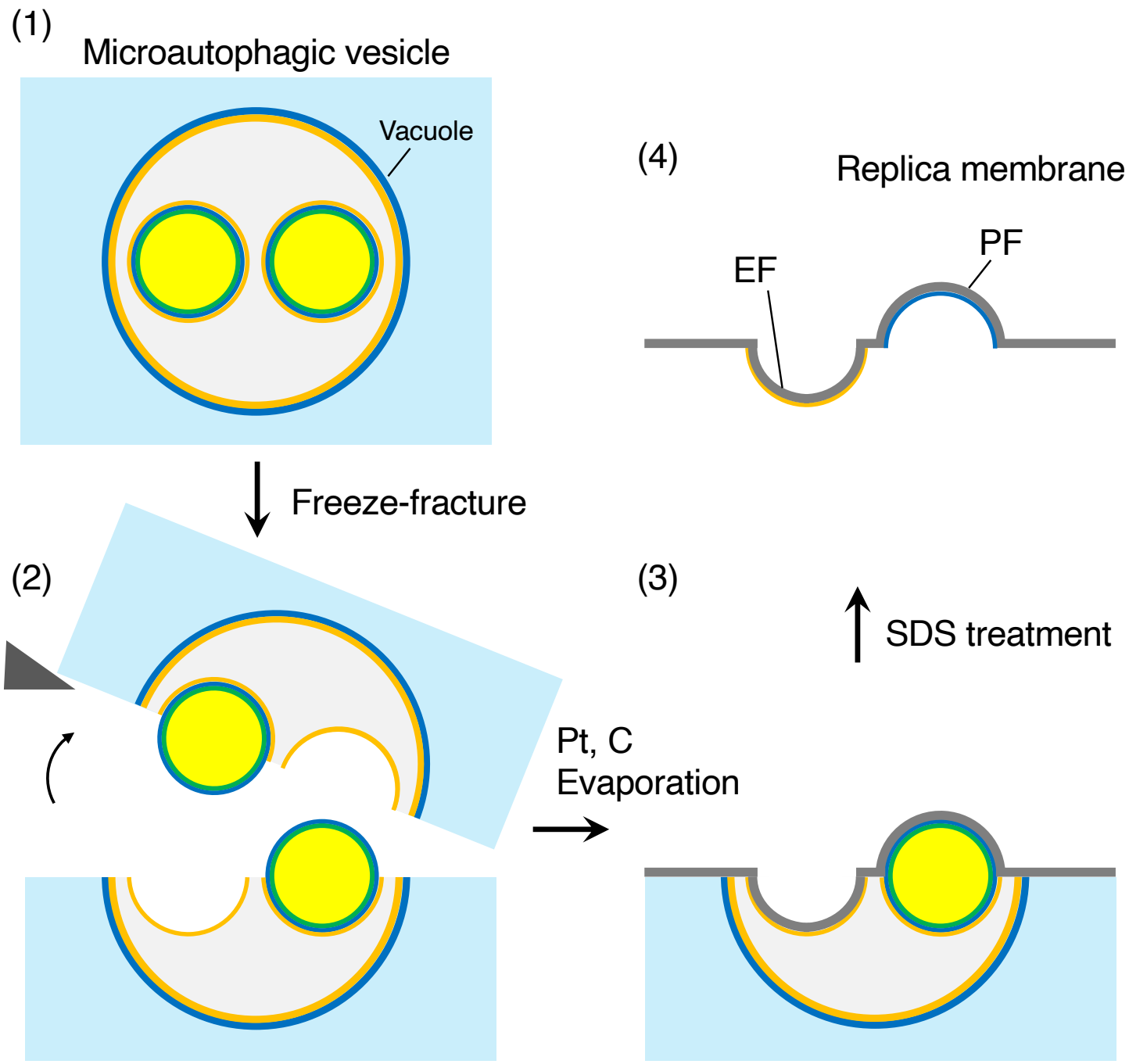
(1)
Microautophagic vesicle
Vacuole
Freeze-fracture
(2)
Pt, C
Evaporation
(3)
SDS treatment
(4)
Replica membrane
EF
PF

Fig. S11

*ubc4*Δ incubated in S(-NC) for 5 hr

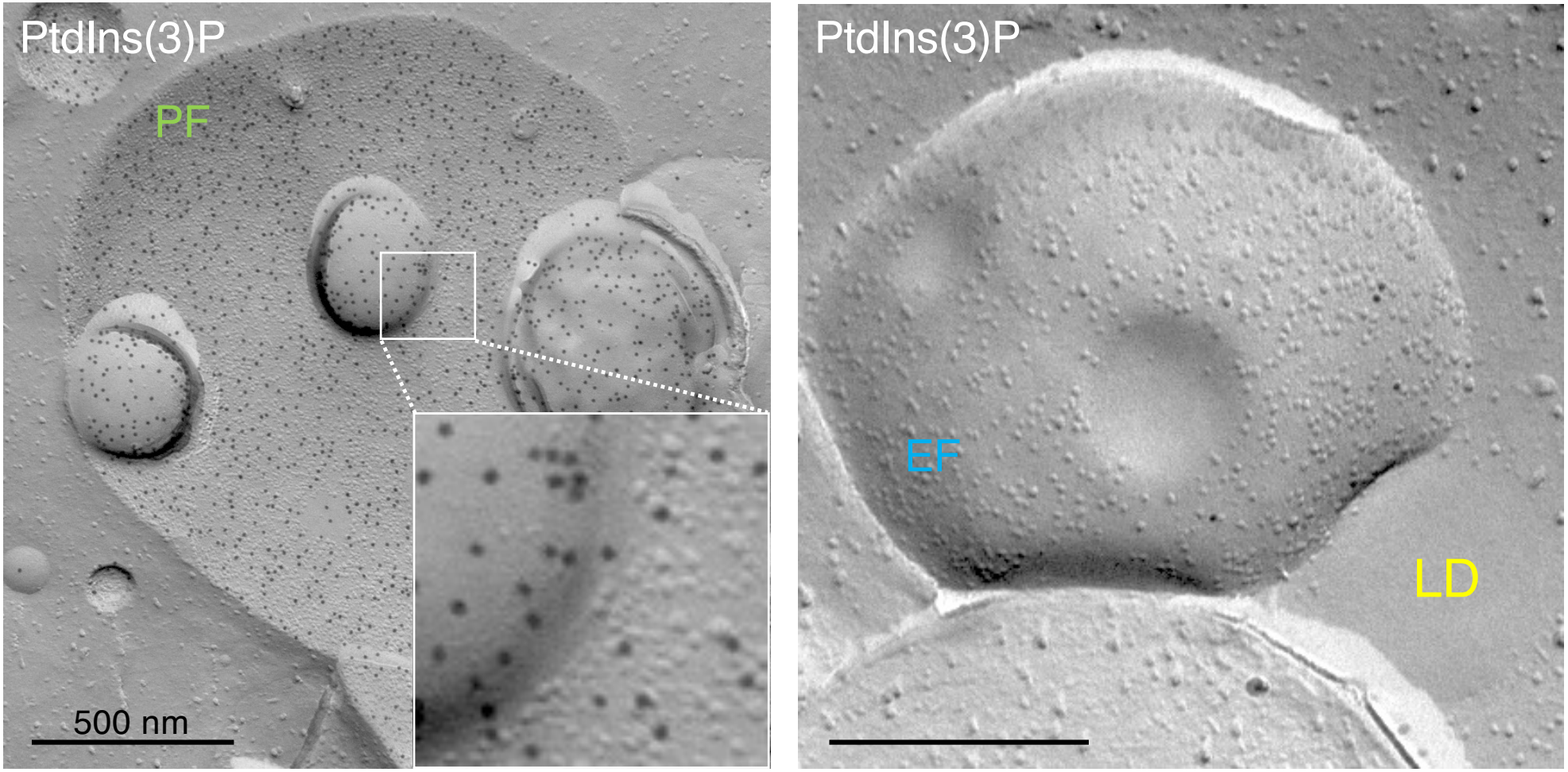

Fig. S12

A PtdEtn in vacuolar membrane

a Starved WT (+Etn)

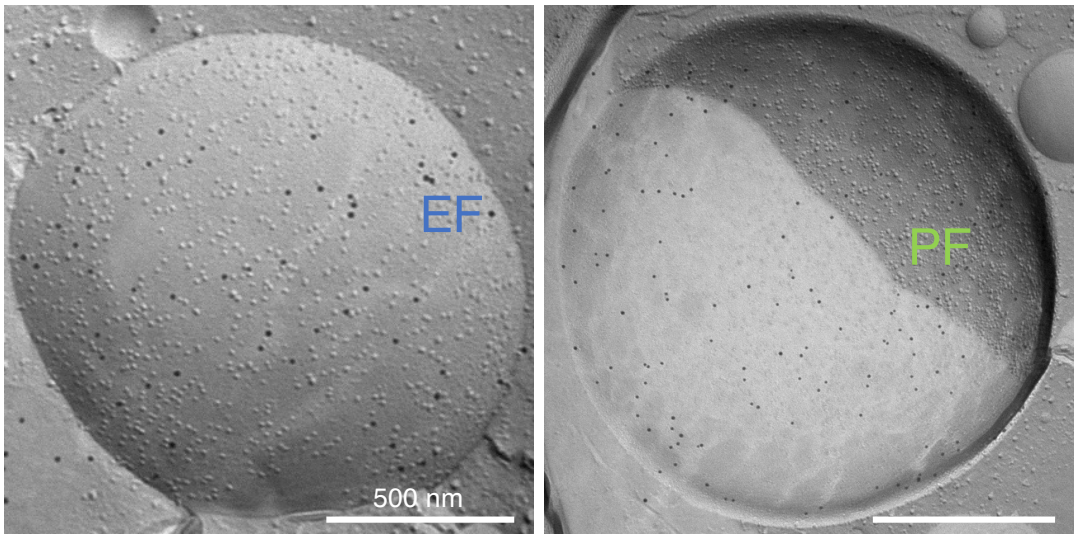

b Starved *cho1*Δ (+Etn)

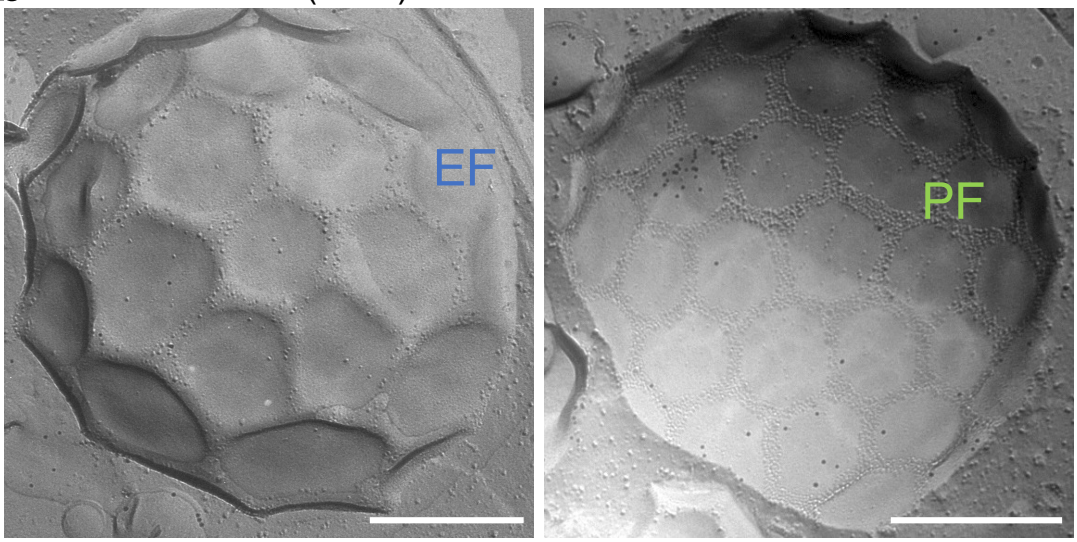

B

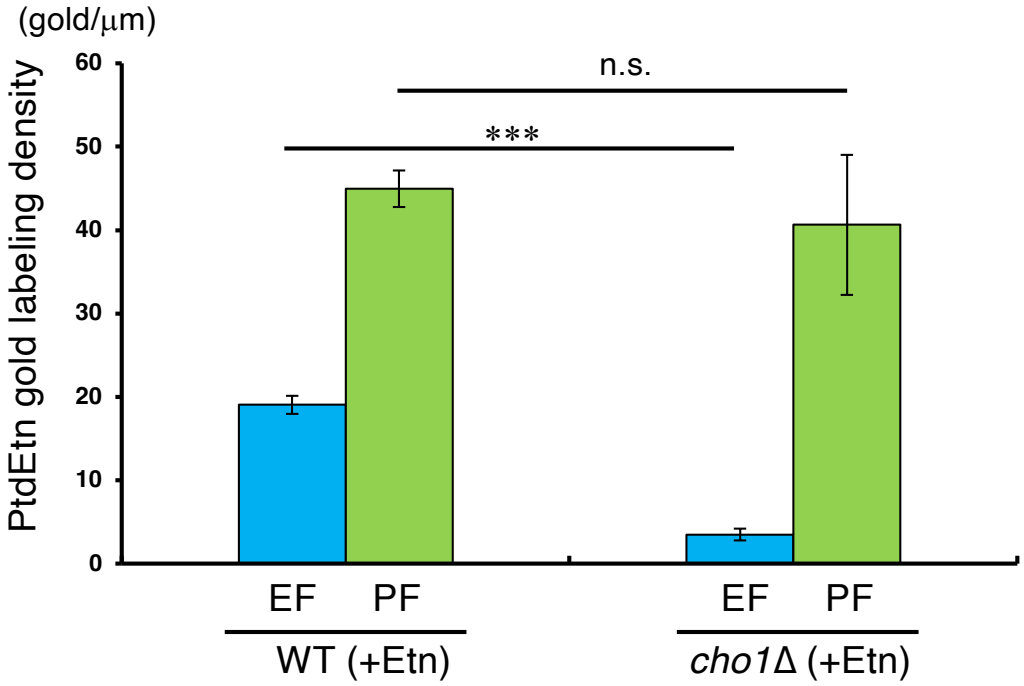

Fig. S13

A Intraluminal vesicles (ILVs) of multi-vesicular body (MVB) in starved *ypt7*Δ mutant

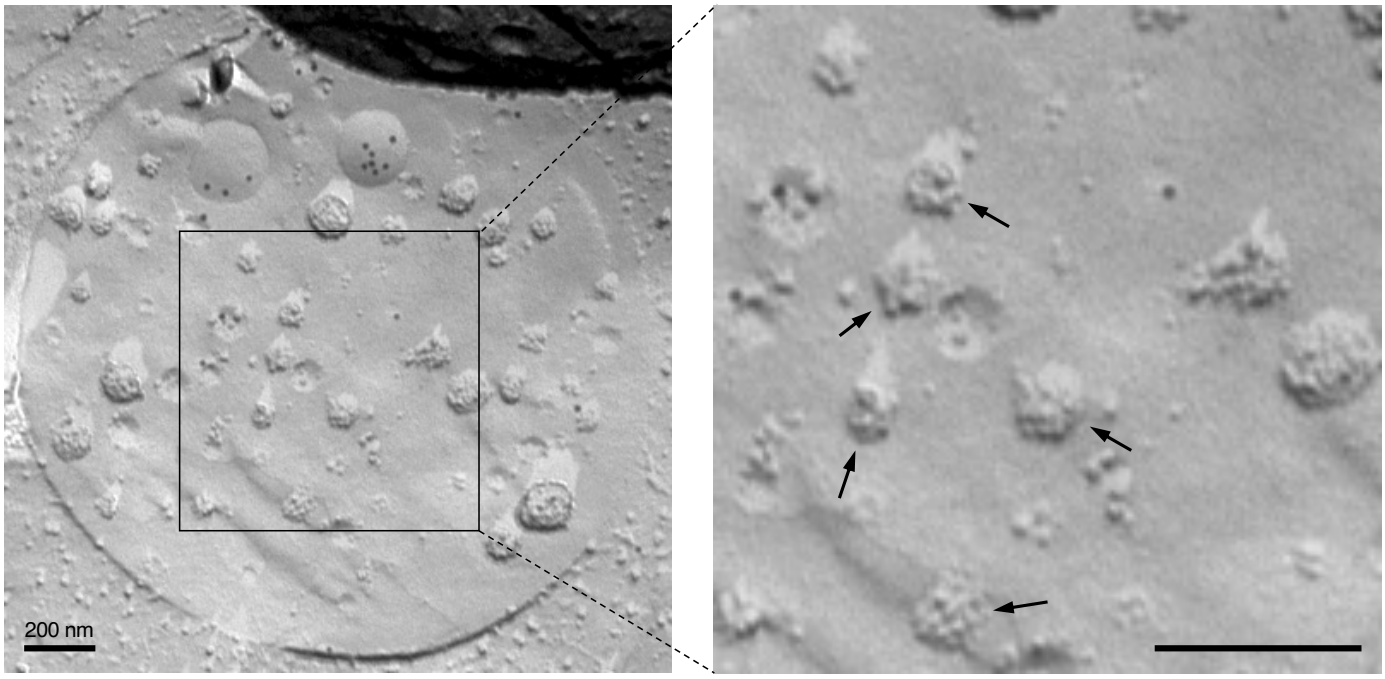

B ILVs of MVB in vacuole of starved *pep4*Δ mutant

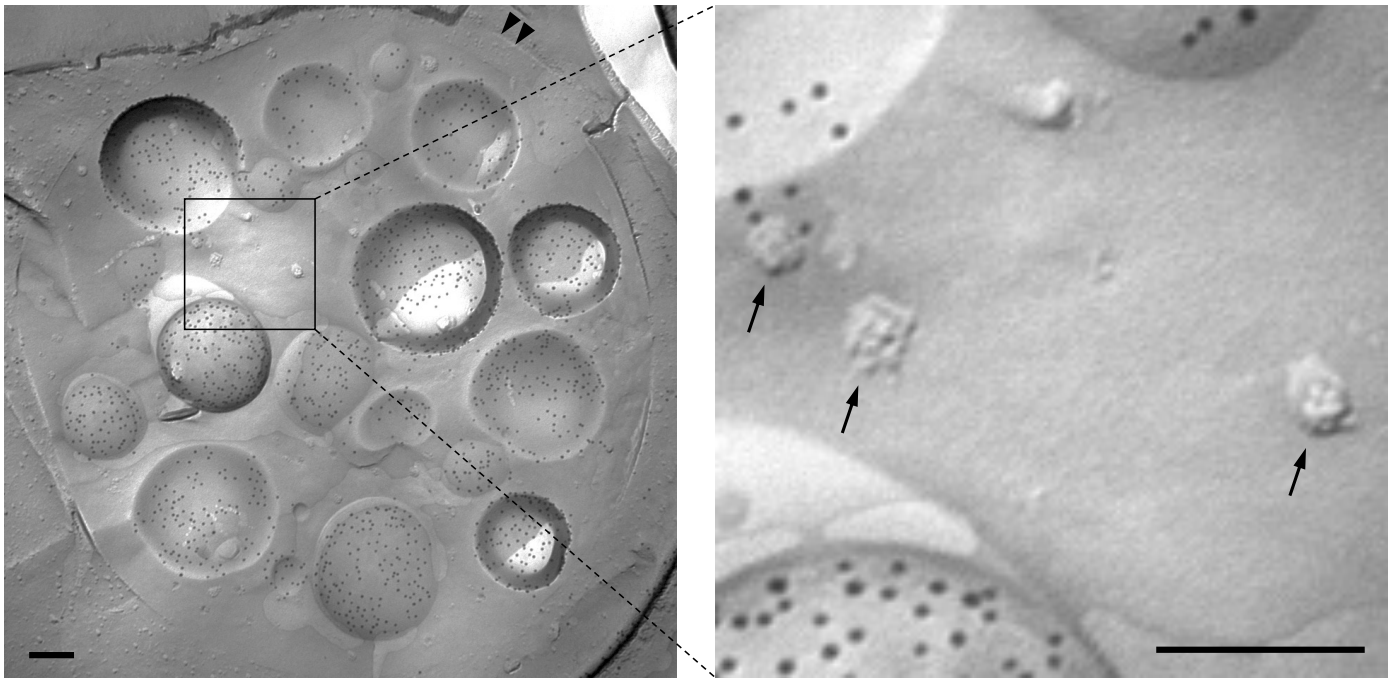

Fig. S14

Name	Genotype	Reference
SEY6210	*MATAα leu2-3, 112 ura3-52 his3-Δ200 trp1-Δ901 lys2-801 suc2Δ9 GAL*	46
AKF002	SEY6210; *ypt7*Δ::KanMX	36
AKF006	SEY6210; *atg4*Δ::KanMX	36
AKF007	SEY6210; *atg2*Δ::KanMX	36
AKF008	SEY6210; *atg3*Δ::KanMX	36
AKF009	SEY6210; *vps34*Δ::KanMX	36
AKF010	SEY6210; *atg7*Δ::KanMX	36
AKF011	SEY6210; *atg8*Δ::KanMX	36
AKF012	SEY6210; *atg9*Δ::KanMX	36
AKF014	SEY6210; *atg12*Δ::KanMX	36
AKF015	SEY6210; *atg16*Δ::KanMX	36
AKF016	SEY6210; *atg18*Δ::KanMX	36
AKF017	SEY6210; *vps15*Δ::KanMX	36
AKF019	SEY6210; *pep4*Δ::KanMX	36
AKF024	SEY6219; *carrying pRS316-GFP-ATG8*	15
AKF044	SEY6210; *cho1*Δ::KanMX	This study
AKF045	SEY6210; *psd1*Δ::KanMX, *psd2*Δ::hphNT1	This study
AKF046	SEY6210; *cho1*Δ::KanMX, *vps27*Δ::hphNT1	This study
AKF047	SEY6210; *cho1*Δ::KanMX *carrying pRS316-GFP-ATG8*	This study
AKF048	SEY6210; *psd1*Δ::KanMX, *psd2*Δ::hphNT1 *carrying pRS316-GFP-ATG8*	This study
AKF050	SEY6210; *cho1*Δ::KanMX, *ubc4*Δ::TRP1	This study
AKF052	SEY6210; *ubc4*Δ::TRP1	This study

Table S1. Yeast strains used in this study.

Deletion mutants were generated using a standard PCR-based method.